PHYSICAL REVIEW D **78,** 114014 (2008)

Treating the *b* quark distribution function with reliable uncertainties

Zoltan Ligeti,[1] Iain W. Stewart,[2] and Frank J. Tackmann[1]

[1]*Ernest Orlando Lawrence Berkeley National Laboratory, University of California, Berkeley, California 94720, USA*
[2]*Center for Theoretical Physics, Massachusetts Institute of Technology, Cambridge, Massachusetts 02139, USA*

(Received 4 August 2008; published 10 December 2008)

The parton distribution function for a b quark in the B meson (called the shape function) plays an important role in the analysis of the $B \to X_s\gamma$ and $B \to X_u\ell\bar{\nu}$ data, and gives one of the dominant uncertainties in the determination of $|V_{ub}|$. We introduce a new framework to treat the shape function, which consistently incorporates its renormalization group evolution and all constraints on its shape and moments in any short distance mass scheme. At the same time it allows a reliable treatment of the uncertainties. We develop an expansion in a suitable complete set of orthonormal basis functions, which provides a procedure for systematically controlling the uncertainties due to the unknown functional form of the shape function. This is a significant improvement over fits to model functions. Given any model for the shape function, our construction gives an orthonormal basis in which the model occurs as the first term, and corrections to it can be studied. We introduce a new short distance scheme, the ''invisible scheme,'' for the kinetic energy matrix element λ_1. We obtain closed form results for the differential rates that incorporate perturbative corrections and a summation of logarithms at any order in perturbation theory, and present results using known next-to-next-to-leading order expressions. The experimental implementation of our framework is straightforward.

DOI: 10.1103/PhysRevD.78.114014 PACS numbers: 13.25.Hw, 11.10.Hi, 12.38.Bx

I. INTRODUCTION

The determination of the Cabibbo-Kobayashi-Maskawa (CKM) matrix element $|V_{ub}|$ from inclusive semileptonic $B \to X_u\ell\bar{\nu}$ decays suffers from large $B \to X_c\ell\bar{\nu}$ backgrounds. In most regions of phase space where this background is kinematically forbidden, the hadronic physics enters via unknown nonperturbative functions, so-called shape functions. At leading order in $\Lambda_{\rm QCD}/m_b$, there is only one such function, which can be extracted from the photon energy spectrum in $B \to X_s\gamma$ [1,2] and used to predict various $B \to X_u\ell\bar{\nu}$ spectra. In $B \to X_s\gamma$ it is the main uncertainty in the effect of the cut on the photon energy, which is near the border of the region where a local operator product expansion (OPE) is applicable. Because of experimental cuts, the shape function is also important for $B \to X_s\ell^+\ell^-$ [3,4].

The determination of $|V_{ub}|$ received renewed attention recently, since the measurement of $\sin 2\beta$ favors a somewhat smaller value of $|V_{ub}|$ than its determination from inclusive decays. One of the most sensitive tests of the standard model flavor sector comes from comparing the sides and angles of the unitarity triangle, so it is important to determine $|V_{ub}|$ with minimal model dependence. Refined calculations of the $B \to X_s\gamma$ rate [5] also provide stringent constraints on new physics.

To obtain $|V_{ub}|$ as precisely as possible, one should combine all existing information on the shape function. The shape function is constrained by the measurements of the shape of the $B \to X_s\gamma$ photon energy spectrum [6–8] and the m_X spectrum in $B \to X_u\ell\bar{\nu}$ [9], and its moments are related to the b quark mass, m_b, and nonperturbative matrix elements of local operators in the OPE, which are constrained by fits to $B \to X_c\ell\bar{\nu}$ decay distributions [10–12]. In addition, the tail of the shape function as well as its renormalization group evolution (RGE) can be calculated perturbatively. A problem is that an arbitrarily small renormalization group running of the shape function develops a perturbative tail whose moments diverge [13].

Currently, there are several approaches to determine $|V_{ub}|$. Often a model for the shape function is chosen, which has a fixed functional form roughly consistent with the $B \to X_s\gamma$ spectrum, and a few adjustable parameters that are fixed by imposing constraints on the first few moments of the shape function. A proposal [14] used by many experimental analyses involves defining moments of the shape function with a cutoff, and a particular procedure to attach a perturbative tail to the model. Unfortunately, there is no clear way to disentangle the shape function and m_b dependencies in this approach, and experimental uncertainties in the shape of the measured $B \to X_s\gamma$ spectrum are not easily incorporated. The issues related to modeling the shape function can be avoided using model independent relations between $B \to X_u\ell\bar{\nu}$ partial rates and weighted integrals of the $B \to X_s\gamma$ spectrum [15–18], which use the measured $B \to X_s\gamma$ spectrum directly as input to predict the $B \to X_u\ell\bar{\nu}$ rates. Although this weighting method allows one to take into account the experimental uncertainties from $B \to X_s\gamma$ straightforwardly, it is hard to combine several measurements, and there is no way to include the additional constraints on m_b and the heavy quark effective theory (HQET) matrix elements. Phase space cuts for which the rate has only subleading depen-

 © 2008 The American Physical Society

dence on the shape function are also possible [19], at the expense of increasing the size of the expansion parameter.

A fully consistent method to combine all experimental constraints on both the shape and moments of the shape function, while also incorporating its known perturbative and nonperturbative behavior, has not yet been given. The framework proposed in this paper provides such a method. It also allows one to obtain reliable error estimates by (i) taking into account all experimental and theoretical uncertainties and correlations and (ii) estimating the uncertainty related to the unknown functional form of the shape function in a systematic fashion.

The shape function $S(\omega, \mu)$ contains nonperturbative physics and obeys the renormalization group equation

$$S(\omega, \mu_i) = \int d\omega' U_S(\omega - \omega', \mu_i, \mu_\Lambda) S(\omega', \mu_\Lambda), \quad (1)$$

where the evolution kernel $U_S(\omega, \mu_i, \mu_\Lambda)$ sums logarithms between the two scales $\mu_i > \mu_\Lambda$. The question is how to determine the function $S(\omega, \mu)$ reliably, which can then be used to extract $|V_{ub}|$ from $B \to X_u \ell \bar{\nu}$, and to analyze $B \to X_s \gamma$ or $B \to X_s \ell^+ \ell^-$ in the low-q^2 region. In Ref. [3] we used the construction

$$S(\omega, \mu_\Lambda) = \int dk C_0(\omega - k, \mu_\Lambda) F(k), \quad (2)$$

where $C_0(\omega, \mu_\Lambda)$ is the b quark matrix element of the shape function operator calculated in perturbation theory, and $F(k)$ is a nonperturbative function that can be extracted from data. Equation (2) has many advantages compared to earlier treatments of the shape function. It ensures that:

(1) $S(\omega, \mu_\Lambda)$ has the correct μ_Λ dependence and RGE.
(2) $S(\omega, \mu_\Lambda)$ has the correct perturbative tail at large ω, while for small ω it is determined by $F(k)$.
(3) The moments of $F(k)$ exist without a cutoff and $F(k)$ falls off exponentially at large k.
(4) Information about matrix elements of local operators in any short distance scheme can be incorporated via constraints on moments of $F(k)$.

A construction similar to Eq. (2) was also used to treat the soft function that describes nonperturbative radiation in jet production in Ref. [20].

The outline of this paper is as follows. In Sec. II we set up our notation and discuss how the shape function enters the decay rates. Our new treatment of the shape function based on Eq. (2) is discussed in Sec. III, including the procedure for incorporating moment constraints in any short distance scheme and an analysis of perturbative corrections in the shape function and decay rate up to two-loop order with a resummation of large logarithms at next-to-next-to-leading-logarithmic (NNLL) order. In Sec. IV we introduce a systematic expansion of $F(k)$ in terms of a suitably chosen set of orthonormal basis functions, which allows one to control the uncertainties arising from its unknown functional form. In Sec. V, we summarize our proposal of how to use all the available data to extract the function $F(k)$ and determine the shape function $S(\omega, \mu)$ with reliable uncertainties, which can then be used for the extraction of $|V_{ub}|$ from $B \to X_u \ell \bar{\nu}$. Section VI contains our conclusions. Details on perturbative corrections and the invisible scheme for the kinetic energy matrix element are summarized in three appendixes.

II. THE $B \to X_s \gamma$ AND $B \to X_u \ell \bar{\nu}$ RATES IN THE SHAPE FUNCTION REGIONS

We use the kinematic variables $p_X^\pm = E_X \mp |\vec{p}_X|$. We also define the partonic variable $p^- = p_X^- + m_b - m_B$. In $B \to X_s \gamma$, $p_X^- = m_B$ $(p^- = m_b)$ and $p_X^+ = m_B - 2E_\gamma$, while in $B \to X_u \ell \bar{\nu}$ they are independent variables with $p_X^+ \le p_X^- \le m_B$. There are three cases where it is known how to carry out a systematic expansion of the decay rate

$$\begin{aligned} &1.\ \text{Nonperturbative shape function:} && \Lambda_{\rm QCD} \sim p_X^+ \ll p_X^-, \\ &2.\ \text{Shape function OPE:} && \Lambda_{\rm QCD} \ll p_X^+ \ll p_X^-, \\ &3.\ \text{Local OPE:} && \Lambda_{\rm QCD} \ll p_X^+ \sim p_X^-. \end{aligned} \quad (3)$$

The region 2 was first studied in $B \to X_u \ell \bar{\nu}$ in Refs. [14,21], and for the $B \to X_s \gamma$ rate in Refs. [22,23]. In the soft collinear effective theory (SCET) regions 1 and 2, where $p_X^+ \ll p_X^-$, the decay rates $\Gamma_s \equiv \Gamma(B \to X_s \gamma)$ and $\Gamma_u \equiv \Gamma(B \to X_u \ell \bar{\nu})$ are given by the factorization theorems [24,25]

$$\begin{aligned} \frac{d\Gamma_s}{dE_\gamma} &= 2\Gamma_{0s} H_s(p_X^+, \mu_i) \\ &\quad \times \int d\omega m_b J(m_b \omega, \mu_i) S(p_X^+ - \omega, \mu_i), \\ \frac{d\Gamma_u}{dE_\ell dp_X^+ dp_X^-} &= \Gamma_{0u} H_u(E_\ell, p_X^-, p_X^+, \mu_i) \\ &\quad \times \int d\omega p^- J(p^- \omega, \mu_i) S(p_X^+ - \omega, \mu_i), \end{aligned} \quad (4)$$

where

$$\Gamma_{0s} = \frac{G_F^2 m_b^5}{8\pi^3} \frac{\alpha_{\rm em}}{4\pi} |V_{tb} V_{ts}^*|^2, \qquad \Gamma_{0u} = \frac{G_F^2 m_b^5}{192\pi^3} |V_{ub}|^2. \quad (5)$$

Corrections are suppressed by $\Lambda_{\rm QCD}/m_b$ and it is known how to include them in Eq. (4). Here we focus on the leading term since the procedure to incorporate the subleading terms follows the same method. The integration limits are implicit in the support of the S and J functions in Eq. (4), which are nonzero when their first argument is positive. Both the hard functions H_u and H_s and the jet function J in Eq. (4) are calculable in a perturbation series in α_s. We summarize results for them in Appendix A up to two-loop order. Only H_u and H_s are process dependent,

and they can sum logarithms between the hard scale and $\mu_i^2 \sim p_X^+ p_X^-$.

The shape function $S(\omega, \mu_i)$ in Eq. (4) sums logarithms between μ_i and μ_Λ through Eq. (1), where in case 1 in Eq. (3) $\mu_\Lambda \sim 1$ GeV, while in case 2 $\mu_\Lambda \sim p_X^+$. In case 1 the shape function is nonperturbative, while in case 2 it can be computed with an OPE to separate the scales $\Lambda_{\rm QCD} \ll p_X^+$. A key feature of Eq. (2) is that it makes the expressions for the decay rates in Eq. (4) simultaneously valid both for cases 1 and 2. For example, it allows an analysis of the photon energy cut in $B \to X_s\gamma$ without having to rely on the expansion in region 2 in $\Lambda_{\rm QCD}/p_X^+$, as was done in Refs. [22,23]. This is important, since in practice, if the momenta in region 2 are not well separated numerically, the utility of expanding in $\Lambda_{\rm QCD}/p_X^+$ is unclear.

It is possible to make Eq. (4) valid for region 3 of Eq. (3), by including appropriate power suppressed and perturbative corrections. At tree level this was carried out in Refs. [26,27], and all results presented below are valid in region 3 at this order. At the level of perturbative corrections these issues were studied in Ref. [28]. We do not include the additional perturbative corrections needed in region 3, since our primary interest is to study the SCET regions 1 and 2. However, it is important that for the perturbative corrections to be correct in region 3, it is required to scale up the different μ's so that $\mu_\Lambda = \mu_i = \mu_b \sim m_b$, because there is only one scale μ in the local OPE. A procedure to carry out this scaling of the μ's is discussed around Eq. (36). A dedicated study of the transition to region 3 is left for future work.

Combining Eqs. (1), (2), and (4), and switching the order of convolutions we arrive at

$$\begin{aligned}\frac{d\Gamma_s}{dE_\gamma} &= 2\Gamma_{0s} H_s(p_X^+, \mu_i) \\ &\quad\times \int dk P(m_b, p_X^+ - k, \mu_i) F(k), \\ \frac{d\Gamma_u}{dE_\ell dp_X^+ dp_X^-} &= \Gamma_{0u} H_u(E_\ell, p_X^-, p_X^+, \mu_i) \\ &\quad\times \int dk P(p^-, p_X^+ - k, \mu_i) F(k).\end{aligned} \tag{6}$$

Here, the perturbatively calculable function P is process independent,

$$\begin{aligned}P(p^-, k, \mu_i) &= \int d\omega \int d\omega' p^- J[p^-(k-\omega), \mu_i] \\ &\quad\times U_S(\omega - \omega', \mu_i, \mu_\Lambda) C_0(\omega', \mu_\Lambda).\end{aligned} \tag{7}$$

At lowest order in perturbation theory

$$P(p^-, k, \mu_i) = \delta(k) + \mathcal{O}(\alpha_s), \tag{8}$$

and the result for P up to $\mathcal{O}(\alpha_s^2)$ with NNLL resummation is given in Appendix A.

Equation (6) can be used to determine the F function by fitting to experimental $B \to X_s\gamma$ and $B \to X_u\ell\nu$ data. We return to this in Sec. V. In the next two sections we explore Eq. (2) in detail and construct a complete orthonormal basis for $F(k)$ that is suitable for carrying out these fits.

III. GENERAL TREATMENT OF THE SHAPE FUNCTION

A. Master formula and OPE constraints

The shape function $S(\omega, \mu)$ is the B meson matrix element

$$S(\omega, \mu) = \langle B|O_0(\omega, \mu)|B\rangle \equiv \langle O_0(\omega, \mu)\rangle_B, \tag{9}$$

of the operator

$$O_0(\omega, \mu) = \bar{b}_v \delta(iD_+ - \delta + \omega) b_v, \tag{10}$$

where we defined

$$\delta = m_B - m_b. \tag{11}$$

Here, b_v is the heavy quark effective theory (HQET) b quark field and $|B\rangle$ is the full QCD B meson state, respectively. (If we used the HQET $|B_v\rangle$ state, this would correspond to absorbing time-ordered products of $O_0(\omega)$ with all power corrections in the HQET Lagrangian into the definition of $S(\omega, \mu)$.) Also, $D_+ = n \cdot D$, v is a timelike vector, and n is a lightlike vector with $n \cdot v = 1$. For our application, $v = p_B/m_B$ is the four-velocity of the B meson, and $\vec{n} = \vec{p}_X/|\vec{p}_X|$ is the direction of the light-quark jet. The μ dependencies of $S(\omega, \mu)$ and $O_0(\omega, \mu)$ are the same. In Eq. (10), our use of $\delta = m_B - m_b$ and the $|B\rangle$ state ensures that $S(\omega, \mu)$ has support for $\omega \geq 0$ with any mass scheme for m_b [27]. Note that δ explicitly depends on the mass scheme. We will use the pole mass scheme first, and discuss converting to short distance schemes in the next subsection.

The information about the shape function that can be obtained from perturbation theory arises from the fact that when integrated over a large enough region, $0 \leq \omega \leq \Lambda$, such that perturbation theory is reliable at the scale Λ, the operator $O_0(\omega)$ can be expanded in a sum of local operators,

$$\begin{aligned}O_0(\omega, \mu) &= \sum_{n=0}^{2} C_n(\omega, \mu) Q_n + \cdots \\ &= \sum_{n=0}^{2} C_n(\omega - \delta, \mu) \tilde{Q}_n + \cdots,\end{aligned} \tag{12}$$

where we use either of the operator bases

$$Q_n = \bar{b}_v (iD_+ - \delta)^n b_v, \qquad \tilde{Q}_n = \bar{b}_v (iD_+)^n b_v. \tag{13}$$

The Wilson coefficients $C_n(\omega)$ for these two bases are equivalent, because $O_0(\omega)$ only depends on the combination $iD_+ - \delta + \omega$. The ellipses in Eq. (12) represent operators of dimension six and higher (where four-quark operators first appear). Taking the B meson matrix element of Eq. (12),

$$S(\omega,\mu)=\sum_{n=0}^{2} C_n(\omega,\mu)\langle Q_n\rangle_B+\cdots, \tag{14}$$

the moments of $S(\omega,\mu)$ with an upper cutoff can be computed

$$\int_0^\Lambda d\omega\,\omega^k S(\omega,\mu)=\sum_n \langle Q_n\rangle_B\int_0^\Lambda d\omega\,\omega^k C_n(\omega,\mu)+\cdots, \tag{15}$$

and are determined by the local matrix elements $\langle Q_n\rangle_B$ plus the perturbative information in the C_n [14]. For the first few matrix elements, we have

$$\langle Q_0\rangle_B=1,\qquad \langle Q_1\rangle_B=-\delta,\qquad \langle Q_2\rangle_B=-\frac{\lambda_1}{3}+\delta^2, \tag{16}$$

where $\lambda_1\equiv\langle B|\bar b_v(iD)^2 b_v|B\rangle$, with the matrix element defined in dimensional regularization. With this definition and the pole mass, the matrix elements in Eq. (16) are μ independent.

The matching coefficients $C_n(\omega,\mu)$ in the OPE in Eq. (12) can be determined at fixed order in perturbation theory by taking a partonic matrix element of both sides of Eq. (12). Consider [21]

$$\begin{aligned}\langle b_v|O_0(\omega+\delta,\mu)|b_v\rangle&=\sum_n C_n(\omega,\mu)\langle b_v|\tilde Q_n|b_v\rangle\\&=C_0(\omega,\mu),\end{aligned} \tag{17}$$

where the b_v states have zero residual momentum, and we used $\langle b_v|\tilde Q_n|b_v\rangle=\delta_{0n}$. The $n\ge 1$ matrix elements vanish in $\overline{\rm MS}$ because there is no dimensionful quantity they can be proportional to. To determine $C_n(\omega,\mu)$ for $n\ge 1$, consider the matrix element between b_v states with residual momentum k^μ where $v\cdot k=0$ but $k_+=n\cdot k\neq 0$. The right-hand side of Eq. (12) gives [21]

$$\begin{aligned}&\langle b_v(k_+)|O_0(\omega+\delta,\mu)|b_v(k_+)\rangle\\&=\langle b_v(0)|O_0(\omega+k_++\delta,\mu)|b_v(0)\rangle\\&=C_0(\omega+k_+,\mu)=\sum_n\frac{k_+^n}{n!}\frac{d^nC_0(\omega,\mu)}{d\omega^n}.\end{aligned} \tag{18}$$

Comparing this with the left-hand side of Eq. (12),

$$\begin{aligned}&\langle b_v(k_+)|O_0(\omega+\delta,\mu)|b_v(k_+)\rangle\\&=\sum_{n=0}^{2} C_n(\omega,\mu)\langle b_v(k^+)|\tilde Q_n|b_v(k^+)\rangle+\cdots\\&=\sum_{n=0}^{2} C_n(\omega,\mu)(k^+)^n+\cdots,\end{aligned} \tag{19}$$

gives for $n=0,1,2$

$$C_n(\omega,\mu)=\frac{1}{n!}\frac{d^nC_0(\omega,\mu)}{d\omega^n}. \tag{20}$$

In Eq. (19), the matrix elements of $\tilde Q_n$ for $n\le 2$ in $\overline{\rm MS}$ are given by their tree-level values k_+^n, because loop graphs have dimension ≥ 1, but are scaleless and vanish.

The coefficients of Q_1 and Q_2 are related by Eq. (20) to the same perturbative coefficient function as Q_0 to all orders in perturbation theory. This is no longer the case at dimension six and higher, where the operator basis includes four-quark operators, and more than one matrix element must be computed.

Our key point is to write the renormalized shape function at the scale μ as in Eq. (2),

$$S(\omega,\mu)=\int dk\,C_0(\omega-k,\mu)F(k), \tag{21}$$

where the function $C_0(\omega,\mu)=\langle b_v|O_0(\omega+\delta,\mu)|b_v\rangle$ has an expansion in α_s and contains perturbatively accessible information about $S(\omega,\mu)$. Equation (21) defines the function $F(k)$, which is a nonperturbative object that can be extracted from data. To see that Eq. (21) uniquely specifies $F(k)$, note that in Fourier space $\tilde S(y,\mu)=\tilde C_0(y,\mu)\tilde F(y)$, so $\tilde F(y)=\tilde S(y,\mu)/\tilde C_0(y,\mu)$.

An important feature of Eq. (21) is that it is consistent with the OPE result in Eq. (14). Expanding its right-hand side in k gives

$$S(\omega,\mu)=\sum_n\frac{1}{n!}\frac{d^nC_0(\omega,\mu)}{d\omega^n}\int dk(-k)^nF(k), \tag{22}$$

and comparing with Eqs. (14) and (20) one finds for $n=0,1,2$

$$\int dk\,k^nF(k)=(-1)^n\langle Q_n\rangle_B. \tag{23}$$

Thus, the first few moments of $F(k)$ are determined by the matrix elements of the local operators $\langle Q_n\rangle_B$, reproducing the OPE for these terms. [The decomposition in Eq. (21) can be extended such that it works for the OPE terms with $n\ge 3$ as well, although we will not do so explicitly here.] Unlike for $S(\omega,\mu)$, for $F(k)$ all moments without a cutoff exist, so $F(k)$ falls faster than any power of k at large k. Furthermore, the characteristic width over which $F(k)$ has substantial support is of order $\Lambda_{\rm QCD}$.

Equation (21) also ensures that $S(\omega,\mu)$ has the correct dependence on μ in the $\overline{\rm MS}$ scheme, since it is determined by $C_0(\omega,\mu)$, which satisfies the shape function RGE in Eq. (1). As shown in Eq. (A23) of Appendix A, a simple formula valid to all orders in α_s can be derived, which combines $S(\omega,\mu_\Lambda)$ from Eq. (21) with the evolution from μ_Λ up to μ_i in Eq. (1),

$$\begin{aligned}S(\omega,\mu_i)&=E_S(\omega,\mu_i,\mu_\Lambda)\\&\quad\times\sum_{j=-1}^{\infty}\sum_{\ell=-1}^{j+1}V_\ell^j(\eta)S_j\Big[\alpha_s(\mu_\Lambda),\frac{\omega}{\mu_\Lambda}\Big]\\&\quad\times\int_0^1 dz\,\mathcal{L}_\ell^\eta(z)F[\omega(1-z)].\end{aligned} \tag{24}$$

Here, $\mathcal{L}_\ell^\eta(z) = [\ln^\ell(z)/z^{1-\eta}]_+$ is defined in Eq. (B9), and S_j, E_S, $\eta = \eta(\mu_i, \mu_\Lambda)$, and $V_\ell^j(\eta)$ are given in Eqs. (A12), (A16), (A17), and (B17), respectively. The S_j coefficients are determined by partonic fixed-order calculations of $C_0(\omega, \mu)$, and at $\mathcal{O}(\alpha_s^2)$ the sum is bounded by $j \le 3$. The RGE factors η and E_S are determined using the anomalous dimensions at various orders. The RGE here has Sudakov double logarithms, implying that the "cusp" anomalous dimension $\Gamma_{\rm cusp}$ must be included at one higher order than the standard anomalous dimensions γ_x. There is no large hierarchy between the scales $\mu_b > \mu_i > \mu_\Lambda$, so the optimal procedure for combining fixed order and resummation is debatable. We adopt the following conventions for our analysis:

$$\begin{aligned} &\text{LL: 1-loop } \Gamma_{\rm cusp}, && \text{tree-level matching;} && \\ &\text{NLL: 2-loop } \Gamma_{\rm cusp}, && \text{1-loop matching,} && \text{1-loop } \gamma_x; \\ &\text{NNLL: 3-loop } \Gamma_{\rm cusp}, && \text{2-loop matching,} && \text{2-loop } \gamma_x. \end{aligned} \tag{25}$$

Our construction ensures that $S(\omega, \mu_i)$ has the correct perturbative tail for large ω, specified by both the constant and logarithmic terms in $C_0(\omega, \mu_i)$, while for small ω it is controlled by the nonperturbative function $F(k)$. Thus Eqs. (21) and (24) build in all the information that can be obtained from considering region 2 in Eq. (3) *without* having to carry out an expansion of the decay rate in this region in $\Lambda_{\rm QCD}/p_X^+$.

A common approach for modeling a parton distribution function is to specify a model for $S(\omega, \mu_\Lambda)$ at a fixed scale μ_Λ and then run it up to a higher μ_i. In this case, μ_Λ must be treated as a model parameter, and changing it can cause significant changes in the model. Furthermore, for $\omega \gg \Lambda_{\rm QCD}$ the perturbative tail of $S(\omega, \mu_i)$ obtained in this approach will not be consistent with carrying out the OPE at μ_i. The perturbative logarithms are reproduced, but the constant terms are not (and the latter are sizable contributions to the OPE for the scales considered here). In Fig. 1 we compare this approach (dashed curves), with the superior approach of describing the shape function via Eq. (24) (solid curves) at NNLL. In each case we use a model for $F(k)$, $\hat{F}^{\rm mod}(k)$ given below in Eq. (34), whose first three moments correspond to $m_b = 4.7$ GeV and $\lambda_1 = -0.31$ GeV^2. The thin dashed curve with the highest peak shows $S(\omega, \mu_i) = \hat{F}^{\rm mod}(\omega)$. The other three dashed curves show the result of fixing $S(\omega, \mu_\Lambda) = \hat{F}^{\rm mod}(\omega)$ at $\mu_\Lambda = 1.0, 1.3, 1.8$ GeV (from bottom to top near the peaks) and running up to $\mu_i = 2.5$ GeV using Eq. (1). The resulting tails at large ω are clearly inconsistent with each other. The solid curves show the result of our approach, using Eq. (24) to obtain $S(\omega, \mu_\Lambda)$ at $\mu_\Lambda = 1.0, 1.3, 1.8, 2.5$ GeV and running up to $\mu_i = 2.5$ GeV. In our approach, $S(\omega, \mu_i)$ is independent of the initial scale μ_Λ, up to subleading corrections in $\alpha_s(\mu_\Lambda)$, and the tails at large ω are consistent with one another. The negative dip at small ω is an artifact of using the pole mass scheme, and will be removed by switching to short distance schemes in the next section. Another feature of the solid curves in Fig. 1 is that their tails become negative for $\omega \gtrsim 2.5$ GeV. It was noted in Ref. [14] that most of this negative tail is canceled by the perturbative corrections from the jet function. We discuss in Sec. III C that this negative tail also disappears if μ_Λ is increased as ω increases.

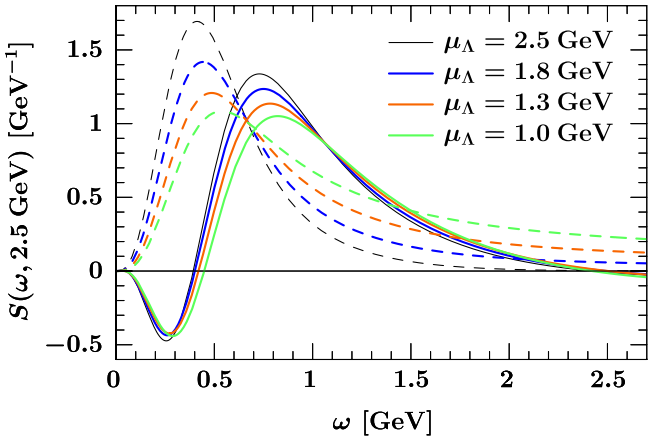

FIG. 1 (color online). Scale independence of our shape function construction. The thin dashed curve with the highest peak shows the model function $S(\omega, \mu_i) = \hat{F}^{\rm mod}(\omega)$ given in Eq. (34). The other dashed curves show the result of taking $S(\omega, \mu_\Lambda) = \hat{F}^{\rm mod}(\omega)$ at $\mu_\Lambda = 1.0, 1.3, 1.8$ GeV (from bottom to top near the peaks) and running up to $\mu_i = 2.5$ GeV with NNLL accuracy. The solid curves use Eq. (24) with $\mu_\Lambda = 1.0, 1.3, 1.8, 2.5$ GeV and running up to $\mu_i = 2.5$ GeV at NNLL. Note the stable tails of the solid curves. The dip at small ω is discussed in the next section.

To obtain the correct perturbative tail, the procedure used in Ref. [28] for $|V_{ub}|$ analyses is to take the perturbative computation of $C_0(\omega, \mu)$ for $\omega \ge \omega_0$ and a model for $S(\omega, \mu)$ for $\omega \le \omega_0$, and these two pieces are glued together, choosing ω_0 so that the result is continuous. The advantage of our construction in Eq. (21) is that the tail automatically turns on in a smooth manner when it dominates over the nonperturbative function $F(k)$ and provides the proper μ dependence for $S(\omega, \mu)$ at any ω.

Imposing the moment constraints on $F(k)$ in Eq. (23) provides a clean way to incorporate the information on the local OPE matrix elements, m_b, λ_1, etc., from $B \to X_c \ell \bar{\nu}$. It is possible to use a shape function scheme in which moments of $S(\omega, \mu)$ with a cutoff define the nonperturbative parameters [14]. Our approach has the advantage of allowing one to use any desired short distance scheme, as we discuss next.

B. Short distance schemes

The most precise information on the matrix elements in Eq. (16) is provided by fitting OPE results to $B \to X_c \ell \bar{\nu}$ decay distributions. This directly constrains $F(k)$ through

Eq. (23). Ideally, we would like to incorporate these constraints on F in a manner that is independent of the order in perturbation theory used to calculate P in Eq. (7). However, if we define the moment parameters δ and λ_1 from Eq. (16) in an infrared sensitive manner such as the pole mass scheme, then the dependence on the order in α_s will not be small—infrared renormalon ambiguities in the perturbation series will cancel against ambiguities in the parameters δ and λ_1. In practice, this means that the values of δ and λ_1 may change substantially when the fit in $B \to X_c \ell \bar{\nu}$ is done at different orders in perturbation theory. In B physics, cancellations between perturbative corrections are significant already at low orders in perturbation theory. Thus, it is preferable to define $F(k)$ and $C_0(\omega, \mu)$ so that they are individually free of renormalon ambiguities, which should make the values of δ and λ_1 more stable to the inclusion of perturbative corrections.

Consider shifting to a new perturbative kernel $\hat{C}_0(\omega, \mu)$ and nonperturbative function $\hat{F}(k)$ that are free from renormalons. To implement this we let

$$C_0(\omega) = \hat{C}_0(\omega) + \delta C_0(\omega), \qquad F(k) = \hat{F}(k) + \delta F(k), \tag{26}$$

such that

$$S(\omega) = \int dk C_0(\omega - k) F(k) = \int dk \hat{C}_0(\omega - k) \hat{F}(k). \tag{27}$$

These shifts move a series of perturbative corrections between $F(k)$ and $C_0(\omega, \mu)$. The shift $\delta F(k)$ will be chosen such that the moments of $\hat{F}(k)$ are given by renormalon-free parameters, and Eq. (27) then determines the corresponding shift $\delta C_0(\omega)$.

We switch from the pole mass m_b and λ_1 to short distance parameters $\hat{m}_b$ and $\hat{\lambda}_1$,

$$m_b = \hat{m}_b + \delta m_b, \qquad \lambda_1 = \hat{\lambda}_1 + \delta\lambda_1, \tag{28}$$

where δm_b and $\delta\lambda_1$ consist of series in $\alpha_s(\mu)$ with the same renormalon as m_b and λ_1, respectively. The freedom to choose these series corresponds to the freedom to choose different schemes for $\hat{m}_b$ and $\hat{\lambda}_1$. To obtain $\hat{F}(k)$ with moments only depending on $\hat{m}_b$ and $\hat{\lambda}_1$, we pick $\delta F(k)$ such that

$$\begin{aligned} \delta F(k) &= F(k) - F(k - \delta m_b) - \Delta F(k), \\ \hat{F}(k) &= F(k - \delta m_b) + \Delta F(k). \end{aligned} \tag{29}$$

Shifting the argument allows us to switch to $\hat{m}_b$. To implement $\hat{\lambda}_1$, $\Delta F(k)$ has to satisfy

$$\begin{aligned} \int dk \Delta F(k) &= \int dk k \Delta F(k) = 0, \\ \int dk k^2 \Delta F(k) &= \frac{\delta\lambda_1}{3}. \end{aligned} \tag{30}$$

The most general solution to Eq. (30) is $\Delta F(k) = (\delta\lambda_1/6) F_1''(k)$, where $F_1(k)$ is an arbitrary function, normalized as $\int dk F_1(k) = 1$.

Using Eqs. (29) and (30) with Eq. (23), one can easily check that $\hat{F}(k)$ has renormalon-free moments, as desired,

$$\begin{aligned} &\int dk \hat{F}(k) = 1, \qquad \int dk k \hat{F}(k) = \delta + \delta m_b = \hat{\delta}, \\ &\int dk k^2 \hat{F}(k) = -\frac{\hat{\lambda}_1}{3} + \hat{\delta}^2, \end{aligned} \tag{31}$$

where $\hat{\delta} = m_B - \hat{m}_b$. Thus the experimental values of the b quark mass and $\hat{\lambda}_1$ extracted in any short distance scheme can be used as inputs in our framework via the moment constraints in Eq. (31).

To determine the corresponding shift in $C_0(\omega)$, we note that Eq. (27) implies $\int dk [C_0(\omega - k)\delta F(k) + \delta C_0(\omega - k)\hat{F}(k)] = 0$. To solve for $\delta C_0(\omega)$, we take the Fourier transform $\delta\tilde{C}_0(y) = -\tilde{C}_0(y)\delta\tilde{F}(y)/\tilde{\hat{F}}(y)$ and thus

$$\delta\tilde{C}_0(y) = \left[1 - e^{iy\delta m_b} - \frac{\delta\lambda_1}{6} y^2 \frac{\tilde{F}_1(y)}{\tilde{\hat{F}}(y)}\right] \tilde{C}_0(y). \tag{32}$$

Here, any $\delta m_b \delta\lambda_1$ cross terms only have higher-order renormalon ambiguities and are dropped. Any choice of $F_1(k)$ is equally good for incorporating the $\delta\lambda_1$ shift. We adopt the simplest choice $F_1(k) = \hat{F}(k)$, which is unique in that it keeps $\hat{C}_0(\omega)$ independent of the precise form of $\hat{F}(k)$.[1] In this case, in momentum space, we have

$$\begin{aligned} \hat{C}_0(\omega) &= C_0(\omega + \delta m_b) - \frac{\delta\lambda_1}{6} \frac{d^2}{d\omega^2} C_0(\omega) \\ &= \left[1 + \delta m_b \frac{d}{d\omega} + \left(\frac{(\delta m_b)^2}{2} - \frac{\delta\lambda_1}{6}\right) \frac{d^2}{d\omega^2}\right] C_0(\omega) \\ &\quad + \cdots, \end{aligned} \tag{33}$$

where $C_0(\omega)$ is determined by the perturbative calculation of $\langle b_v | O_0(\omega + \delta, \mu) | b_v \rangle$, and the ellipsis denotes terms that are either $\mathcal{O}(\alpha_s^3)$ or beyond the order we are working at for the moments of $\hat{F}(k)$. The same strategy to determine $\hat{F}(k)$ and derive the corresponding $\hat{C}_0(\omega)$ can be applied to higher moments if in the future terms with $n \geq 3$ in Eq. (23) are included in the analysis.

In the remainder of this paper we use the convolution formula for $S(\omega, \mu)$ in terms of $\hat{C}_0(\omega, \mu)$ and $\hat{F}(k)$ in Eq. (27). We shall regard $\hat{F}(k)$ as the fundamental nonperturbative object to be extracted from data. In particular,

[1]There are other possible choices. For example, taking $F_1(k) \propto k^2 \hat{F}(k)$ would ensure that the $\delta\lambda_1$ shift does not change the small-k behavior of $\hat{F}(k)$. However, if $F_1(k) \neq \hat{F}(k)$, the shift $\delta C_0(\omega)$ depends on $\hat{F}(k)$, and must be recomputed each time $\hat{F}(k)$ changes. Hence other choices are more difficult to implement when performing a fit to data to extract $\hat{F}(k)$.

TABLE I. Central values of the input parameters. The last three entries are computed from m_b^{1S} and λ_1 at order α_s^2.

Parameter	Value
$\alpha_s(m_Z)$ [29]	0.1176
$\alpha_s(4.7\ \mathrm{GeV})$	0.2155
m_B	5.279 GeV
m_b^{1S} [12]	4.70 GeV
λ_1 [12]	$-0.31\ \mathrm{GeV}^2$
λ_1^{i}	$-0.32\ \mathrm{GeV}^2$
$m_b^{\mathrm{kin}}(1\ \mathrm{GeV})$	4.57 GeV
$\lambda_1^{\mathrm{kin}}(1\ \mathrm{GeV})$	$-0.47\ \mathrm{GeV}^2$

in Sec. IV we will build a complete basis of functions for $\hat{F}(k)$.

C. Numerical results for $S(\omega, \mu)$

To illustrate the effect of using our method to include the perturbative corrections to the shape function through $\hat{C}_0$ we choose a model for $\hat{F}(k)$,

$$\hat{F}^{\mathrm{mod}}(k) = \frac{1}{\lambda}\Big[\sum_{n=0}^{2} c_n f_n\Big(\frac{k}{\lambda}\Big)\Big]^2. \tag{34}$$

Here $\lambda = 0.8$ GeV, $f_n(x)$ is given below in Eq. (48), and the three parameters c_0, c_1, and c_2 are fixed to satisfy the constraints in Eq. (31) for the appropriate short distance scheme. For our numerical analysis we use the input values collected in Table I. With $\{m_b^{1S}, \lambda_1\}$ we have $\{c_0, c_1, c_2\} = \{0.949, -0.309, 0.064\}$, while for $\{m_b^{1S}, \lambda_1^{\mathrm{i}}\}$ we have $\{c_0, c_1, c_2\} = \{0.949, -0.307, 0.075\}$, and for $\{m_b^{\mathrm{kin}}, \lambda_1\}$ we have $\{c_0, c_1, c_2\} = \{0.988, -0.120, -0.095\}$.

First, we switch from the pole mass to a short distance mass. We use the $1S$ mass [30] and the kinetic mass [31] schemes,

$$\hat{\delta} \equiv \delta^{1S} = m_B - m_b^{1S}, \qquad \hat{\delta} \equiv \delta^{\mathrm{kin}} = m_B - m_b^{\mathrm{kin}}, \tag{35}$$

to fix the first moment in Eq. (31), and λ_1 to determine the second moment. The choice of mass scheme enters $\hat{C}_0(\omega)$ through the δm_b and $\delta\lambda_1$ in Eq. (33), which must be expanded in α_s to avoid the renormalons. Details of the implementation of short distance schemes and the expressions for δm_b^{1S} and $\delta m_b^{\mathrm{kin}}$ are discussed in Appendix A 3. In Fig. 2 we show the result for $S(\omega, \mu_i)$ obtained from $C_0(\omega, \mu_\Lambda)$ with $\mu_\Lambda = 1.3$ GeV, run up to $\mu_i = 2.5$ GeV at next -to-leading logarithmic (NLL) order (dashed) and NNLL order (solid). The dark, medium, and light curves show the results in the pole $1S$ and kinetic mass schemes, respectively. In both short distance mass schemes the negative dip present in the pole scheme is removed, while the perturbative tail at large ω remains unchanged. The removal of the negative dip is similar to what was observed for the soft function for jets in Ref. [20].

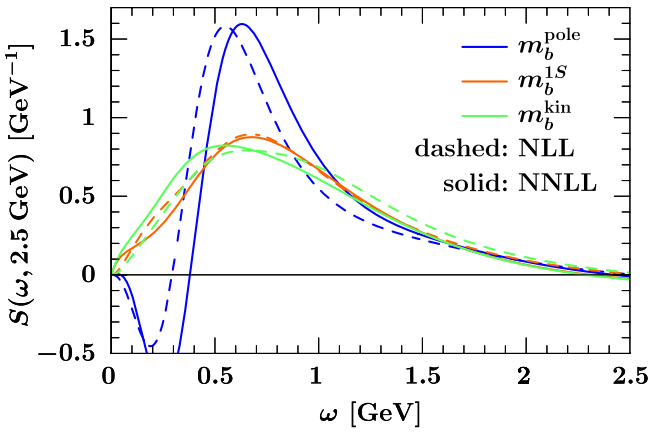

FIG. 2 (color online). $S(\omega, \mu_i)$ obtained from $\hat{C}_0(\omega, \mu_\Lambda)$ with $\mu_\Lambda = 1.3$ GeV and run up to $\mu_i = 2.5$ GeV at NLL (dashed) and NNLL (solid) order. Shown are results using the pole mass scheme and the $1S$ and kinetic short distance mass schemes. Switching to the short distance schemes, the result becomes more stable going from NLL to NNLL, the negative dip at small ω in the pole scheme is removed, while the perturbative tail at large ω remains unchanged.

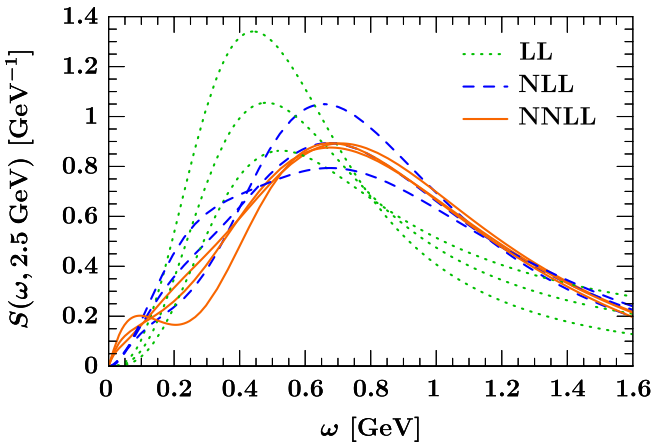

FIG. 3 (color online). μ_Λ dependence of $S(\omega, 2.5\ \mathrm{GeV})$ in the peak region obtained from $\hat{C}_0(\omega, \mu_\Lambda)$ at LL (dotted), NLL (dashed), and NNLL (solid) order, using m_b^{1S} and λ_1. The three curves in each case are for $\mu_\Lambda = 1.0, 1.3, 1.8$ GeV. The μ_Λ dependence is significantly reduced at each higher order.

In Fig. 3 we illustrate the perturbative convergence and residual μ_Λ scale dependence of the result of Eq. (24) order by order, using the $1S$ mass scheme and λ_1. We show $S(\omega, \mu_i = 2.5\ \mathrm{GeV})$ run up from μ_Λ at leading logarithmic (LL) (dotted), NLL (dashed) and NNLL (solid). For each order, the three curves correspond to $\mu_\Lambda = 1.0, 1.3, 1.8$ GeV. As expected, the μ_Λ dependence is significantly reduced by going from LL to NLL to NNLL. For the lowest scale, $\mu_\Lambda = 1.0$ GeV, an oscillation begins to build up at small ω, which is clear at NNLL where the curves for the two larger scales are quite stable. Although we continue to explore μ_Λ as low as 1.0 GeV in

this section, we take this as evidence that slightly larger values of μ_Λ should be used to ensure a convergent expansion for $\hat{C}_0$. Therefore, we will use $\mu_\Lambda = 1.2, 1.5, 1.9\,\text{GeV}$ in Sec. III D for the decay rate.

Next, we switch to short distance schemes for λ_1. Note that the NLL results in Fig. 2 with λ_1 defined in dimensional regularization are already quite stable. Unlike for the pole mass, there is not much numerical evidence for the importance of switching to a short distance scheme for λ_1, and adding a sizable $\delta\lambda_1 \sim \mathcal{O}(\alpha_s)$ correction may oversubtract. The $u = 1$ renormalon in λ_1 is related to the large-order behavior of perturbation theory, and it is unclear how much numerical impact it has on the perturbative coefficients computed at $\mathcal{O}(\alpha_s)$ and $\mathcal{O}(\alpha_s^2)$. In Appendix C we show that schemes with $\delta\lambda_1 = \mathcal{O}(\alpha_s)$ appear to oversubtract, causing large oscillations in the shape function at small ω. This is shown explicitly for the kinetic scheme $\lambda_1^{\text{kin}}(= -\mu_\pi^2)$. Therefore, in Appendix C we introduce a new short distance scheme with $\delta\lambda_1 = \mathcal{O}(\alpha_s^2)$, which we call the invisible scheme and denote by λ_1^{i}. The expression for $\delta\lambda_1^{\text{i}}$ is given in Eq. (A37). In this short distance scheme, the NLL results are unchanged. In Fig. 4 we compare results at NNLL for m_b^{1S} and λ_1 versus using m_b^{1S} and λ_1^{i}. One sees that the invisible scheme has only a small effect on the NNLL shape function, which is entirely at small ω. It damps the oscillation that occurs when $\mu_\Lambda = 1.0$ GeV and modifies the slope.

In Fig. 5 we show the μ_Λ scale dependence at NLL (dashed) and NNLL (solid) order in the tail region. The lower six curves use the same scale variation as in Fig. 3. Here, as one uses the SCET expansion, but enters the local OPE region, the scale dependence increases with ω, and the tail becomes negative. This is due to increasing $\ln(\omega/\mu_\Lambda)$ terms, for which the above choices of μ_Λ are inappropriate. To avoid potentially large logarithms, we

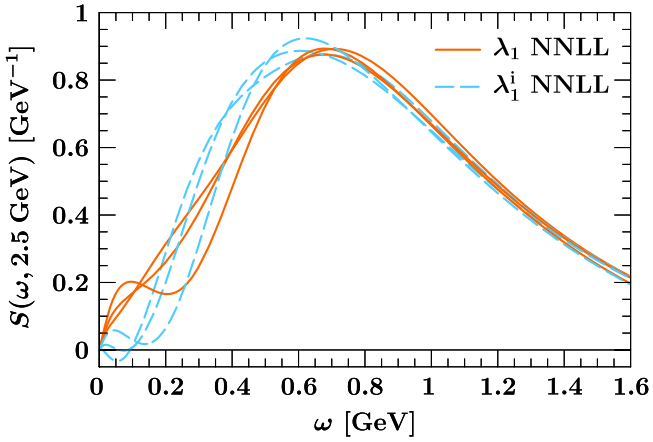

FIG. 4 (color online). The effect of using the invisible scheme for λ_1 on $S(\omega, 2.5\,\text{GeV})$ at NNLL order. The solid lines are the same as those in Fig. 3, using m_b^{1S} and λ_1, while the dashed lines use m_b^{1S} together with λ_1^{i}. The three curves in each case are for the same values of μ_Λ as in Fig. 3.

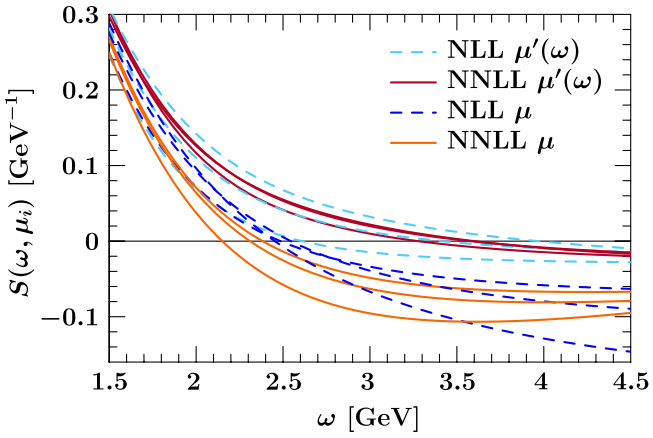

FIG. 5 (color online). μ_Λ dependence of $S(\omega, 2.5\,\text{GeV})$ in the tail region (lower six curves) and of $S(\omega, \mu_i')$ (upper six curves) at NLL (dashed) and NNLL (solid) order, using m_b^{1S} and λ_1^{i}. For the lower six curves we vary $\mu_\Lambda = 1.0, 1.3, 1.8\,\text{GeV}$, while for the upper ones we use the running scale parameters $\mu_\Lambda'(\omega)$ in Eq. (36) and $\mu_i'(\omega)$ described in the text.

can increase μ_Λ as we increase ω by taking, for example,

$$\mu_\Lambda'(\omega) = a + b\arctan(\omega - 2.5\ \text{GeV}). \tag{36}$$

To vary the scales, we take three functions of this form, with a and b chosen such that for $\omega = 0$ they give $\mu_\Lambda' = 1.0, 1.3, 1.8$ GeV and for $\omega = 4.7$ GeV they give $\mu_\Lambda' = 2.35, 4.7, 9.4$ GeV. In Fig. 5, the six upper curves show $S(\omega, \mu_i)$ obtained with these $\mu_\Lambda'(\omega)$ choices, taking $\mu_i = \mu_i'(\omega) = [\mu_\Lambda'(\omega) m_b^{1S}]^{1/2}$ with the central $\mu_\Lambda'(\omega)$. Comparing the upper and lower curves shows that increasing μ_Λ with ω significantly reduces the μ_Λ scale dependence to a similar level as in the peak region shown in Fig. 3. (We have checked that using the running $\mu_\Lambda'(\omega)$ does not have an effect on the size of the scale uncertainty in the peak region.) The upper curves in Fig. 5 also have a much less negative tail, which is caused predominantly by increasing μ_Λ with ω, and only partially by increasing the reference scale μ_i. This means that the dominant part of the negative tail in the lower curves is caused by large logarithms of ω/μ_Λ. Hence, increasing μ_Λ with ω will be important to obtain a positive rate in the tail region. The importance of increasing μ with a kinematic variable in the tail region was also pointed out for jet production in Ref. [32], where it was required to avoid a negative tail for the cross section.

In the decay rate the μ_i dependence of $S(\omega, \mu_i)$ cancels against corrections from the jet function, so the intermediate scale μ_i should also run with increasing ω. This is accomplished by taking $\mu_i = \mu_i'(\omega) = [\mu_\Lambda'(\omega)\mu_b]^{1/2}$ for each of the three running $\mu_\Lambda'(\omega)$'s from Eq. (36). This treatment of the tail has the advantage that we obtain $\mu_\Lambda = \mu_i = \mu_b$ for $\omega \sim m_b$, and by construction the standard factor of 2 scale variation, $m_b/2 < \mu_b < 2m_b$. Hence it

is consistent with the local OPE treatment for region 3 in Eq. (3). The rate at which equality is approached can be controlled by multiplying the argument of the arctan in Eq. (36) by a scaling factor, and the center of the transition region can be adjusted by modifying the 2.5 GeV value shown there.

D. Perturbative results for the $B \to X_s\gamma$ spectrum

In this section we explore the scale dependence of the perturbative corrections to the $B \to X_s\gamma$ spectrum in the SCET regions 1 and 2 in Eq. (3). The rate depends on three scale parameters $\mu_\Lambda \gtrsim 1$ GeV, $\mu_i \sim \sqrt{m_b\Lambda_{\rm QCD}}$, and $\mu_b \sim m_b$. In a short distance scheme the decay rate in Eq. (6) becomes

$$\frac{d\Gamma_s}{dp_X^+} = \Gamma_{0s} H_s(p_X^+, \mu_b) U_H(m_b, \mu_b, \mu_i) \times \int dk \hat{P}(m_b, k, \mu_i) \hat{F}(p_X^+ - k), \qquad (37)$$

where H_s and U_H are given in Eqs. (A1) and (A14), and the notation $\hat{P}$ and $\hat{F}$ indicate that these are given in a short distance scheme. From the analysis in Appendix A, all perturbative corrections can be organized into a simple series of plus distributions $\mathcal{L}_j^\eta(z)$, defined in Eqs. (B9) and (B10). The integral of the perturbative function P with the F function is then

$$\int dk P(p^-, k, \mu_i) F(p_X^+ - k) = \sum_{j=-1}^{\infty} P_j(p^-, p_X^+, \mu_i, \mu_\Lambda) \int_0^1 dz \mathcal{L}_j^\eta(z) F[p_X^+(1-z)], \qquad (38)$$

where explicit results for the coefficients P_j are given in Eq. (A25). The additional terms generated by transforming Eq. (38) into the integral over the short distance $\hat{P}$ and $\hat{F}$ are described in detail in Appendix A 3.

In Figs. 6–8, we study the μ_Λ, μ_i, and μ_b dependencies of the p_X^+ spectrum for $B \to X_s\gamma$, namely $(d\Gamma_s/dp_X^+)/[\Gamma_{0s}|C_7^{\rm incl}(0)|^2]$. Recall that this has a simple relation to the photon energy spectrum $p_X^+ = m_B - 2E_\gamma$. We show the p_X^+ spectrum to facilitate easier comparison with the results for the shape function in the previous section. Since we are interested in studying the perturbative corrections, we keep $\hat{F}^{\rm mod}(k)$ fixed to be our default model in Eq. (34). In each of Figs. 6–8, we show results at LL (dotted curves), NLL (dashed curves), and NNLL (solid curves) order, for three different values of the scales, and using the $1S$ mass and λ_1^i scheme. The central values are $\mu_\Lambda = 1.5$ GeV, $\mu_i = 2.5$ GeV, and $\mu_b = 4.7$ GeV, two of which are held fixed in each plot. In Fig. 6 the three curves at each order show $\mu_\Lambda = 1.2, 1.5, 1.9$ GeV, in Fig. 7 they show $\mu_i = 2.0, 2.5, 3.0$ GeV, and in Fig. 8

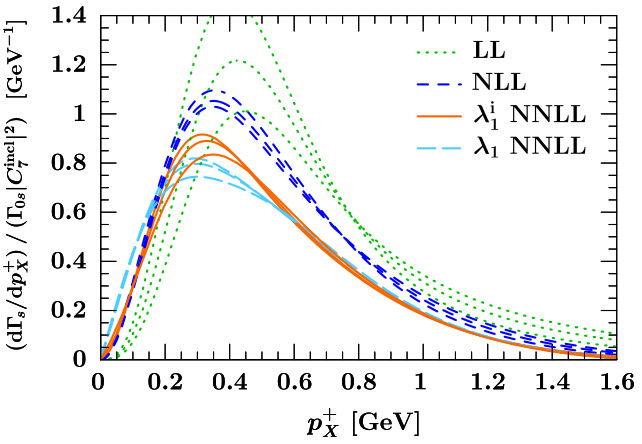

FIG. 6 (color online). μ_Λ dependence of the $B \to X_s\gamma$ spectrum in terms of m_b^{1S} and λ_1^i, using $\hat{F}^{\rm mod}(k)$. Shown are the LL (dotted), NLL (dashed), and NNLL (solid) spectra for $\mu_\Lambda = 1.2, 1.5, 1.9$ GeV. The long dashed curves are the NNLL spectra with m_b^{1S} and λ_1, showing less convergence at small ω.

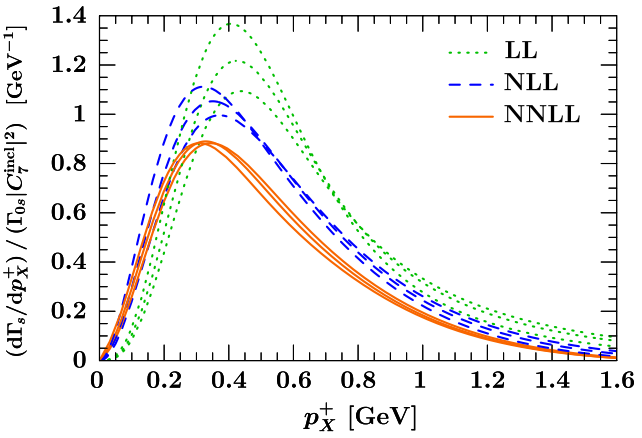

FIG. 7 (color online). μ_i dependence of the $B \to X_s\gamma$ spectrum in terms of m_b^{1S} and λ_1^i, using $\hat{F}^{\rm mod}(k)$, at LL (dotted), NLL (dashed), and NNLL (solid) order for $\mu_i = 2.0, 2.5, 3.0$ GeV.

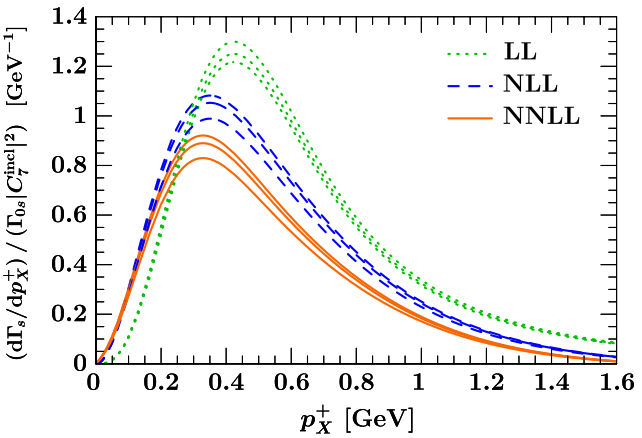

FIG. 8 (color online). μ_b dependence of the $B \to X_s\gamma$ spectrum in terms of m_b^{1S} and λ_1^i, using $\hat{F}^{\rm mod}(k)$, at LL (dotted), NLL (dashed), and NNLL (solid) order for $\mu_b = 2.35, 4.7, 9.4$ GeV.

they show $\mu_b = 2.35, 4.7, 9.4$ GeV. Since the scales should obey the hierarchy $\mu_\Lambda < \mu_i < \mu_b$, it is not possible to vary each by a factor of 2. For illustration, we do vary μ_b by a factor of 2, but keep μ_Λ and μ_i in ranges suitable to the physical shape function and jet function regions, respectively. The largest effect going from LL to NLL to NNLL is the change in the normalization. Although it is not captured by our range of scale variation, the normalization still exhibits reasonable convergence. Rescaled to a common normalization, the shape of the spectrum shows very nice convergence, and the range of scales used is clearly suitable here. We find a reduction in the scale dependence order by order for most values of p_X^+.

In Fig. 6 we show three additional NNLL curves (long dashed) that use m_b^{1S} and λ_1 instead of $\lambda_1^{\rm i}$. Comparing these curves to the solid curves (m_b^{1S} and $\lambda_1^{\rm i}$), we see that the overall effect of using $\lambda_1^{\rm i}$ instead of λ_1 is small. However, one can clearly observe that the invisible scheme improves the perturbative convergence of the spectrum at small p_X^+.

Although we do not show results here for the spectrum in the local OPE region 3 in Eq. (3), we checked that the same effects as in the tail of $S(\omega, \mu_i)$ in Fig. 5 appear in the tail of the spectrum. To avoid a large μ_Λ dependence in the tail, the scales must be increased with ω as discussed below Eq. (36), and this also helps to obtain a positive tail for the spectrum in region 3.

It is important to emphasize that in the common approach to model distribution functions corresponding to the dashed curves in Fig. 1, where a fixed model for $S(\omega, \mu_\Lambda)$ is specified at the scale μ_Λ and then run up to μ_i, the spectrum will have a large dependence on μ_Λ, which must be considered a model parameter. Thus, there is no analog to the μ_Λ independence of the rate obtained in our construction, and illustrated in Fig. 6. Note that the dependence of the $B \to X_s\gamma$ rate for $p_X^+ \le (p_X^+)^{\rm cut}$ on the soft and intermediate scales μ_Λ and μ_i has so far been studied only by performing an expansion in $\Lambda_{\rm QCD}/(p_X^+)^{\rm cut}$ in region 2 of Eq. (3) [22,23], as in Eqs. (12) and (14). In this case, one can combine the same perturbative ingredients as in our approach, depending on the three scales μ_Λ, μ_i, and μ_b. As mentioned before, the advantage of our framework is that it does not rely on performing an expansion in region 2.

IV. EXPANSION OF THE F FUNCTION

A. Complete orthonormal basis

So far in the literature the uncertainty related to the unknown functional form of the shape function has been either neglected or estimated by using a few model functions for $S(\omega, \mu)$, and varying their parameters or distorting them [3,28,33,34], subject to constraints on their first few moments. To obtain a systematic estimate of the uncertainty related to the unknown functional form of the shape function, we construct a suitable set of complete orthonormal basis functions for the function $\hat{F}(k)$ defined by Eq. (27). The uncertainty in the functional form is then determined by the uncertainty in the coefficients of this basis. This expansion will also be convenient to extract $\hat{F}(k)$ from experimental data, including experimental and theoretical uncertainties and correlations.

Since $\hat{F}(k)$ has mass dimension -1, it is convenient to introduce a dimension-one parameter λ and use the dimensionless variable $x = k/\lambda$. By power counting, $\lambda \sim \Lambda_{\rm QCD}$. We expect on physical grounds that $\hat{F}(k)$ is positive, so we can expand its square root,

$$\hat{F}(\lambda x) = \frac{1}{\lambda}\Big[\sum_{n=0}^{\infty} c_n f_n(x)\Big]^2, \tag{39}$$

where $f_n(x)$ are a complete set of orthonormal functions,

$$\int_0^\infty dx f_m(x) f_n(x) = \delta_{mn}. \tag{40}$$

Since $\hat{F}(k)$ is normalized to unity, the coefficients c_n satisfy

$$1 = \int dk \hat{F}(k) = \int dx \Big[\sum_n c_n f_n(x)\Big]^2 = \sum_n c_n^2. \tag{41}$$

Although $\hat{F}(k)$ is independent of the choice of basis functions $f_n(x)$ when summing over all n, in practice only a finite number of terms can be kept. Therefore, we want to choose basis functions $f_n(x)$ such that the first few terms in Eq. (39) provide a good approximation to $\hat{F}(k)$. Unfortunately, most of the well-known orthonormal functions on $[0, \infty)$ become broader with increasing n, and hence have moments whose values increase with n [35]. By dimensional analysis, the n-th moment of $\hat{F}(k)$ scales as $\Lambda_{\rm QCD}^n$, and we would like the basis functions to satisfy this constraint, at least for the low-n moments.

To construct a suitable orthonormal basis $f_n(x)$ on $[0, \infty)$, we consider orthonormal functions $\phi(y)$ on $[-1, 1]$ and a variable transformation $y(x)$, which maps $x \in [0, \infty)$ to $y \in [-1, 1]$. We choose $y(x)$ to be increasing, $y'(x) > 0$. Then, for any orthonormal basis $\phi_n(y)$ on $[-1, 1]$,

$$f_n(x) = \sqrt{y'(x)}\,\phi_n[y(x)] \tag{42}$$

provides an orthonormal basis on $x \in [0, \infty)$. Choosing different ϕ_n's and different $y(x)$'s allows us to change the basis functions. It is natural to choose $\phi_n(y)$ to be polynomials of degree n, and we find it convenient to use the normalized Legendre polynomials

$$\phi_n(y) = \sqrt{\frac{2n+1}{2}} P_n(y), \qquad P_n(y) = \frac{1}{2^n n!}\frac{d^n}{dy^n}(y^2 - 1)^n. \tag{43}$$

To determine $y(x)$, note that for a positive definite function $Y(x)$, such that $\int_0^\infty dx Y(x) = 1$, the function

$$y(x) = -1 + 2\int_0^x dx' Y(x'), \tag{44}$$

satisfies $y(0) = -1$ and $y(\infty) = +1$. Since $y'(x) = 2Y(x)$, the first basis function is simply

$$[f_0(x)]^2 = y'(x)\phi_0^2[y(x)] = Y(x). \tag{45}$$

To obtain a good approximation to $\hat{F}(k)$ with the first few terms in Eq. (39), one should choose $Y(x)$ to be "similar" to $\lambda\hat{F}(\lambda x)$. This gives an intuition about suitable choices, and once $Y(x)$ and λ are fixed, the full basis is specified. A convenient choice for $Y(x)$ is

$$Y(x, p) = \frac{(p+1)^{p+1}}{\Gamma(p+1)} x^p e^{-(p+1)x} \tag{46}$$

for any $p > 0$ real parameter. Constructing a basis from $Y(x, p)$ yields basis functions for which the first and second moments of $f_m(x)f_n(x)$ are order one or smaller. Therefore, the terms in the expansion in Eq. (39) have n-th moments of order λ^n or smaller. Choosing the scaling parameter $\lambda \sim \Lambda_{\rm QCD}$, the first few terms in the expansion in the resulting basis gives a good approximation to the shape function.

The function in Eq. (46) is similar to those used to model $S(\omega, \mu)$ in the literature. In fact, by choosing $Y(x)$ to be a specific model shape function, our construction allows one to expand about it, and systematically study corrections to an assumed functional form. We emphasize, however, that in our approach the only role of $\phi_n(y)$ and $Y(x)$ is to specify the basis functions $f_n(x)$. The functional form for $Y(x)$ affects how quickly the expansion in Eq. (39) converges, but not the fact that it is a convergent expansion. The completeness of the basis $\phi_n(y)$ on $[-1, 1]$ implies that any square integrable function on $[0, \infty)$ can be expanded in terms of the bases $f_n(x)$ resulting from the above construction.

Using Eq. (46) gives basis functions that behave as $f_n^2(x) \sim x^p$ as $x \to 0$. Because of the short distance subtractions in Eq. (33), to ensure that $S(\omega, \mu)$ goes to zero at $\omega = 0$, we need $\hat{F}(k)$ to go to zero at least as k^3 for $k \to 0$. Thus, we find it convenient to use $Y(x, 3)$ as our default choice, with

$$y(x, 3) = 1 - 2\left(1 + 4x + 8x^2 + \frac{32}{3}x^3\right)e^{-4x}, \tag{47}$$

which gives the orthonormal functions

$$f_n(x) = 8\sqrt{\frac{2x^3(2n+1)}{3}}e^{-2x}P_n[y(x, 3)]. \tag{48}$$

For numerical calculations we use $\lambda = 0.8$ GeV as default.

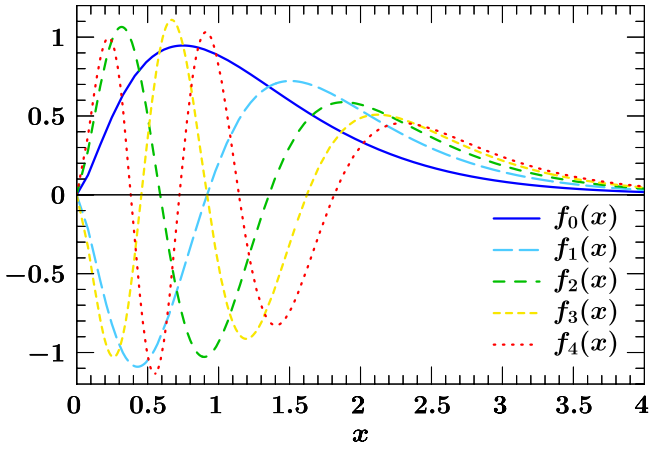

FIG. 9 (color online). The first five orthonormal basis functions in Eq. (48).

These functions are also convenient because they allow analytic calculations of the decay spectra. The first five basis functions in Eq. (48) are shown in Fig. 9. In Fig. 10 we use these to illustrate the uncertainty remaining in $\hat{F}(k)$ if its first three moments are fixed. We fix c_3 and c_4 to nine different combinations, and choose the first three coefficients $c_{0,1,2}$ to satisfy the moment constraints in Eq. (31). All the nine functions shown have $0.92 < c_0 < 0.95$, $-0.35 < c_1 < -0.28$, and $0.01 < c_2 < 0.14$. Even this plot makes the uncertainties look smaller than they are, since at small k the k^3 behavior of these models appears to imply a small uncertainty. Including the short distance subtractions from Eq. (33), these models yield a significantly wider variation in $S(\omega, \mu)$ for small ω. Figure 10 shows that even with small errors of the $B \to X_c \ell \bar{\nu}$ moments, more information on the shape function can be extracted from the $B \to X_s\gamma$ or $B \to X_u \ell \bar{\nu}$ data.

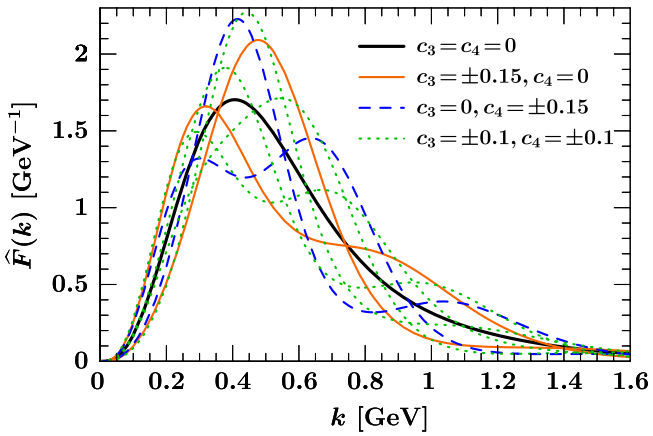

FIG. 10 (color online). Nine functions with identical first three moments. For each curve, we fix c_3 and c_4 and then choose c_0, c_1, c_2 to satisfy the moment constraints in Eq. (31) with m_b^{1S} and λ_1^i. The thick solid curve ($c_3 = c_4 = 0$) corresponds to the default model used in Sec. III.

B. Truncation uncertainties

Equation (39) provides a model independent description of $\hat{F}(k)$ for any choice of the basis. Since the basis is complete for any value of λ, we will regard λ along with the function $Y(x)$ as part of the convention that defines the basis. In practical applications one has to truncate the series in Eq. (39) after the first $N+1$ terms,

$$\hat{F}^{(N)}(k) \equiv \frac{1}{\lambda}\Big[f^{(N)}\Big(\frac{k}{\lambda}\Big)\Big]^2 = \frac{1}{\lambda}\Big[\sum_{n=0}^{N} c_n f_n\Big(\frac{k}{\lambda}\Big)\Big]^2 = \frac{1}{\lambda}\sum_{m,n=0}^{N} c_m c_n f_m\Big(\frac{k}{\lambda}\Big) f_n\Big(\frac{k}{\lambda}\Big), \tag{49}$$

and use $\hat{F}^{(N)}(k)$ in the actual calculations.

Figure 11 illustrates how the expansion converges. Both plots show a toy Gaussian model function (thick solid curve), which we expand in terms of the first n basis functions in Eq. (48) for $n \le 4$. In the top panel, we use the default value $\lambda = 0.8$ GeV to define the basis. The truncated series in Eq. (49) quickly approaches the model function, even for small values of N. In the bottom panel, we show the same expansion using $\lambda = 0.6$ GeV to define the basis, which illustrates how the value of λ affects the convergence of the expansion.

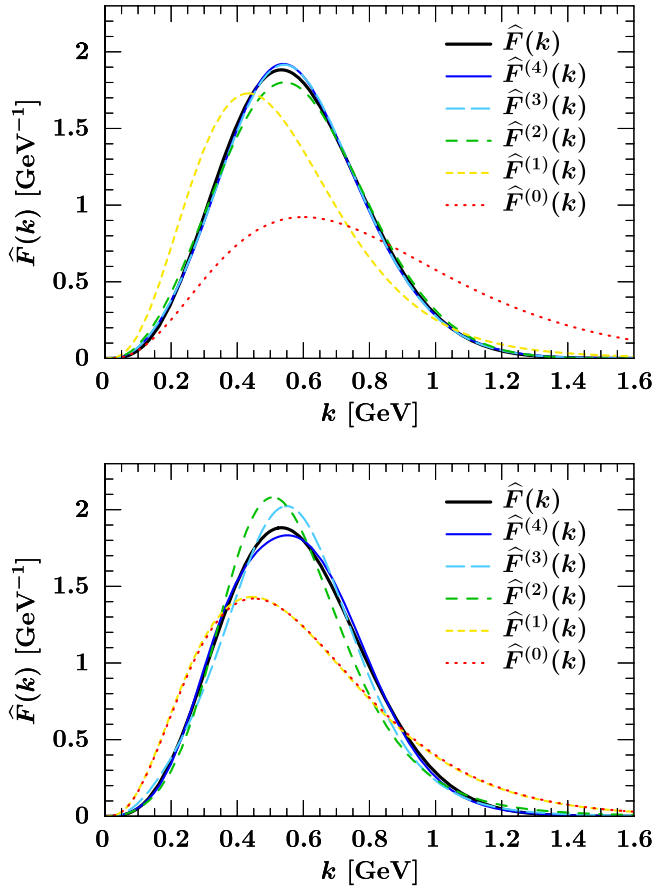

FIG. 11 (color online). Top: expansion of a Gaussian model function $\hat{F}^{\rm Gauss}(k) = (2/a)(k/a)^3 \exp[-(k/a)^2]$ with $a = 0.639$ GeV, corresponding to $m_b = 4.7$ GeV, using the first five basis functions $f_n(x)$ in Eq. (48). Bottom: same as on the top, except that in the definition of the basis λ is changed from 0.8 GeV to 0.6 GeV.

To quantify the uncertainties, we would like to have a systematic way to estimate the error due to the neglected terms in the truncated sum in Eq. (49). The truncation error is affected by the choice of N, $Y(x)$, and λ, providing several handles on this uncertainty. A virtue of adding one more term from our orthonormal basis, compared to adding one more parameter to a generic model, is that due to the orthogonality of the basis functions the additional parameter provides independent information and should avoid large parameter correlations. By varying N, one can change the number of coefficients, and study how sensitive the results are to the truncation. As a consistency check, one can use a different basis, or change $Y(x)$ or λ, and check that the difference is within the previous truncation error estimate.

A feature of our construction is that the truncation error can be estimated using $\sum_{n=0}^{\infty} c_n^2 = 1$. We define

$$\sqrt{\lambda \hat{F}(\lambda x)} \equiv f(x) = f^{(N)}(x) + c_r f_r(x), \tag{50}$$

where

$$c_r = \Big(1 - \sum_{n=0}^{N} c_n^2\Big)^{1/2}, \tag{51}$$

and the remainder function $f_r(x)$ is orthogonal to $f_{0,\ldots,N}(x)$,

$$f_r(x) = \sum_{n=1}^{\infty} r_n f_{N+n}(x), \tag{52}$$

and normalized

$$\int_0^\infty dx [f_r(x)]^2 = 1, \qquad \sum_{n=1}^{\infty} r_n^2 = 1. \tag{53}$$

In terms of $f_r(x)$, the truncation error from approximating $\hat{F}(k)$ by $\hat{F}^{(N)}(k)$ is

$$\hat{F}^{(N)}_{\rm trunc}[f_r](k) \equiv |\hat{F}(k) - \hat{F}^{(N)}(k)| = \frac{1}{\lambda}\Big|2c_r f_r\Big(\frac{k}{\lambda}\Big) f^{(N)}\Big(\frac{k}{\lambda}\Big) + c_r^2 f_r^2\Big(\frac{k}{\lambda}\Big)\Big|. \tag{54}$$

Although Eq. (53) implies $|r_n| \le 1$, it provides no bound on $\sum_n |r_n|$. Therefore, one cannot derive a rigorous bound on $|f_r(x)|$ from Eq. (52) for all $x > 0$, and it is not possible to obtain a rigorous bound on the truncation error $\hat{F}^{(N)}_{\rm trunc}$ either. However, for practical purposes, it is sufficient to estimate $\hat{F}^{(N)}_{\rm trunc}$. Its size is controlled by c_r in Eq. (51), which is determined by the first $N+1$ coefficients, and can be minimized by choosing a good basis. Thus, as long as enough coefficients are included in the basis so that the

estimated truncation uncertainty is small compared to other uncertainties, any reasonable estimate of $f_r(x)$ provides a useful estimate of the truncation uncertainty.

For suitable choices of the basis, we expect the series to converge fairly quickly, since the higher basis functions oscillate more and more rapidly, and we do not expect significant structure in the momentum distribution of the b quark in the B meson over momentum scales $\ll \Lambda_{\rm QCD}$. Hence, one way to estimate $f_r(x)$ is to assume that one term in Eq. (52) saturates the sum. It is natural to take that to be the first (possibly the second) term, which corresponds to

$$f_r(x) = \pm f_{N+1}(x). \tag{55}$$

Another possibility is to assume that $|f_r(x)| \lesssim f_0(x)$ and take

$$f_r(x) = \pm f_0(x). \tag{56}$$

This is motivated by the fact that, except for small and large values of x, $f_0(x)$ gives roughly an envelope for the higher basis functions, as can be seen from Fig. 9. In each case, the sign of $f_r(x)$ is undetermined. For small c_r, the second term in Eq. (54) can be neglected and the sign of $f_r(x)$ is irrelevant.

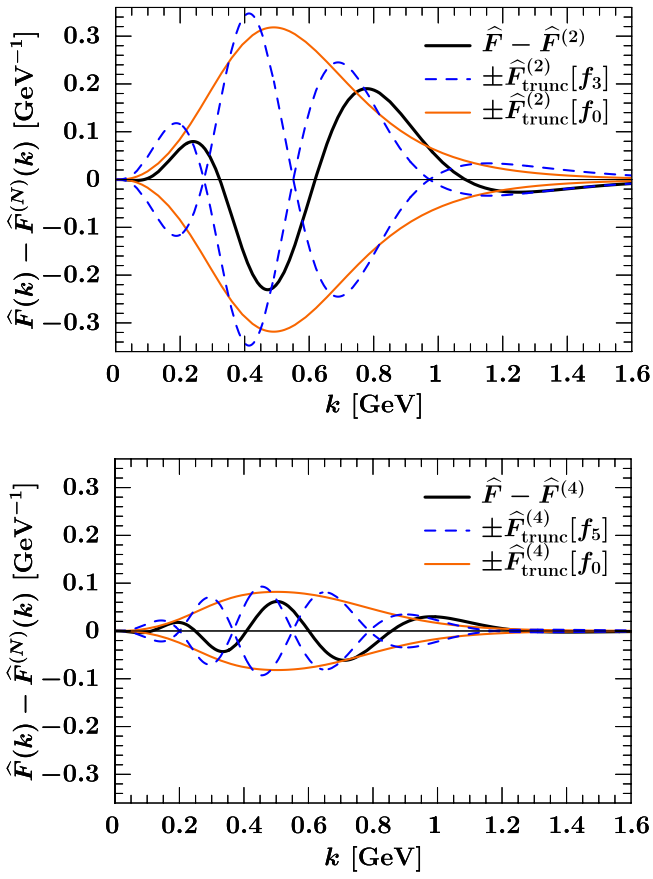

FIG. 12 (color online). Truncation error estimates. The thick solid curves show $\hat{F}^{\rm Gauss}(k) - \hat{F}^{(N)}(k)$ corresponding to the bottom plot in Fig. 11, for $N = 2$ (top) and $N = 4$ (bottom). The dashed curves show $\pm\max\{\hat{F}^{(N)}_{\rm trunc}[\pm f_{N+1}]\}$, and the thin solid curves show $\pm\max\{\hat{F}^{(N)}_{\rm trunc}[\pm f_0]\}$, i.e., the error estimates using Eqs. (55) and (56), respectively.

To illustrate these methods for estimating the truncation error we consider again the toy model used in Fig. 11, with $\lambda = 0.6$ in our basis as in the bottom panel. In Fig. 12, the thick solid curve shows $\hat{F}(k) - \hat{F}^{(N)}(k)$ for $N = 2$ (top panel) and $N = 4$ (bottom panel). The dashed curves show the estimate using Eq. (55), taking the point-by-point maximum of $\hat{F}^{(N)}_{\rm trunc}[\pm f_{N+1}](k)$, while the thin solid curves use Eq. (56) instead. As expected, the former correlates more with the absolute value of the point-by-point deviations, while the latter roughly envelopes the difference. As can be seen, we obtain reasonable estimates of the deviation of $\hat{F}^{(N)}(k)$ from $\hat{F}(k)$. The overall sizes of the truncation errors are well estimated in both plots, because they are proportional to c_r. For the top plot $c_r = 0.088$ and for the bottom plot $c_r = 0.025$. If the expansion of $\hat{F}(k)$ converges reasonably fast, then $f_r(x)$ will be an oscillatory function, as shown in Fig. 12. Ultimately we are interested in how the shape function impacts the uncertainty in the extraction of $|V_{ub}|$ or that in determining the $B \to X_s\gamma$ event fraction above a certain photon energy cut. These depend on weighted integrals of $\hat{F}(k)$, so their uncertainties will be much smaller than the point-by-point errors in approximating $\hat{F}(x)$ by $\hat{F}^{(N)}(x)$ shown in Fig. 12.

C. Subleading shape functions

Any precision analysis of differential spectra in $B \to X_s\gamma$ or $B \to X_u\ell\bar{\nu}$ must incorporate power corrections that go beyond Eq. (4). At order $\Lambda_{\rm QCD}/m_b$, six subleading shape functions enter the description of the most general inclusive spectra in $B \to X_s\gamma$ and $B \to X_u\ell\bar{\nu}$ [36–39]. We refer to these as the primary subleading shape functions. In addition there are terms in $B \to X_s\gamma$ that enter from operators other than O_7 and are related to the photon's hadronic structure, whose contribution to the total rate is not calculable in the OPE [40,41]. Considering only the primary subleading shape functions and using suitably weighted integrals of the $B \to X_u\ell\bar{\nu}$ differential rate together with $B \to X_s\gamma$, the $\mathcal{O}(\Lambda_{\rm QCD}/m_b)$ shape functions can be canceled in the determination of $|V_{ub}|$ [42]. However the same drawbacks apply to the weighting method at subleading order as those mentioned already in the introduction, so it is interesting to consider how our analysis can be extended to include these subleading shape functions.

The appropriate factorization theorem for the primary subleading shape functions, analogous to Eq. (4), is known from Ref. [39]. Thus, when one-loop partonic calculations of these functions and their corresponding jet functions are available, a construction analogous to Eq. (21) can be carried out to build in the proper large-ω tail, μ_Λ dependence, etc. However, it should be cautioned that a large

number of additional shape functions enter in the matching at $\mathcal{O}(\alpha_s\Lambda_{\rm QCD}/m_b)$ [39,43,44], so the utility of extending our full analysis to this level is unclear.

Here, we simply discuss how a complete basis can be constructed for the primary subleading shape functions. We know less about these shape functions than about the leading order one. Their moments are still related to HQET matrix elements. In particular, the zeroth moment of the $\mathcal{O}(\Lambda_{\rm QCD}/m_b)$ shape functions vanishes, which means they must be negative for some values of k, and their first moments either vanish or are given by linear combinations of λ_1 and λ_2. The zeroth moments no longer vanish for the $\mathcal{O}(\Lambda_{\rm QCD}^2/m_b^2)$ shape functions and beyond [26,27,37].

For simplicity, we define the sign of each $\mathcal{O}(\Lambda_{\rm QCD}/m_b)$ shape function such that its first nonzero moment is positive. A convenient expansion for the functions with vanishing first moment is given by

$$H(\lambda x) = -\frac{d}{dx}\Big[\sum_n d_n f_n(x)\Big]^2, \tag{57}$$

while the four-quark operator shape functions, whose zeroth and first moments vanish, can be expanded as

$$H^{4q}(\lambda x) = \frac{d^2}{dx^2}\Big[\sum_n d_n f_n(x)\Big]^2. \tag{58}$$

With this form, $\int_0^\infty dk H^{(4q)}(k) = \int_0^\infty dk k H^{4q}(k) = 0$. The first nonzero moments provide constraints on the coefficients, similar to Eq. (41), for example

$$\int_0^\infty dk k H(k) = \lambda^2 \sum_n d_n^2, \tag{59}$$

which can be set to the appropriate linear combinations of λ_1 and λ_2. Note that a different set of coefficients d_n occurs for each subleading shape function.

V. EXTRACTING THE F FUNCTION AND PREDICTING DECAY RATES

For a given basis for the leading and subleading shape functions we want to extract the basis coefficients c_i and d_i, including their uncertainties and correlations. This extraction will use data on the $B \to X_s\gamma$ and $B \to X_u\ell\bar\nu$ spectra and data that determines moments of the shape functions from $B \to X_c\ell\bar\nu$. To simplify our discussion, we adopt a notation that is suitable for the coefficients $\{c_0, \ldots, c_N\}$ of the function $\hat F(k)$ appearing in the leading shape function. The generalization to incorporate subleading shape functions is straightforward. All results in this section are exact for $N \to \infty$ and for finite N one has to take into account the truncation error discussed in Sec. IV B.

Since the function $\hat F(k)$ enters the decay spectra linearly, we can independently compute the contributions of the product of any two basis functions $f_m(x)f_n(x)$ in the expansion of $\hat F(k)$, which we denote by $d\Gamma_{mn}$. The differential spectra $d\Gamma_s = d\Gamma_s/dE_\gamma$ or $d\Gamma_u = d\Gamma_u/dE_\ell dp_X^+ dp_X^-$ are then given by

$$d\Gamma = \sum_{m,n=0}^{N} c_m c_n d\Gamma_{mn}, \tag{60}$$

where from combining Eq. (6) and (39), the $d\Gamma_{mn}$ are

$$d\Gamma_{mn} = \Gamma_0 H(p^-) \times \int_0^{p_X^+} dk \frac{\hat P(p^-,k)}{\lambda} f_m\Big(\frac{p_X^+ - k}{\lambda}\Big) f_n\Big(\frac{p_X^+ - k}{\lambda}\Big). \tag{61}$$

For simplicity, we suppress the scale μ in the arguments of H and $\hat P$, and the u or s subscripts on H. The $d\Gamma_{mn}$ in Eq. (61) act as a basis for the physically measurable distributions, and the result in Eq. (60) is a quadratic polynomial in each of the fit parameters c_i.

In practice, experimental spectra are binned. Integrating Eq. (60) the rate in the i-th bin is

$$\Gamma^i = \sum_{m,n=0}^{N} c_m c_n \Gamma^i_{mn}, \tag{62}$$

where Γ^i_{mn} is the integral of $d\Gamma_{mn}$ in Eq. (61) over the phase space region of the i-th bin. In addition, we can impose constraints on the moments of $\hat F(k)$,

$$M^j = \int_0^\infty dk k^j \hat F(k) = \sum_{m,n=0}^{N} c_m c_n M^j_{mn}. \tag{63}$$

Here, M^j are given in terms of experimental measurements of $\hat\delta$ and $\hat\lambda_1$ from $B \to X_c\ell\bar\nu$, while M^j_{mn} is

$$M^j_{mn} = \frac{1}{\lambda}\int_0^\infty dk k^j f_m\Big(\frac{k}{\lambda}\Big) f_n\Big(\frac{k}{\lambda}\Big). \tag{64}$$

One can determine the coefficients $\{c_0, \ldots, c_N\}$ by fitting Eqs. (62) and (63) to the experimental data. It is straightforward to combine several different spectra and measurements by different experiments. Doing a simultaneous fit to Eqs. (62) and (63) allows one to combine the $B \to X_s\gamma$ shape information [6–8] and information on the m_X spectrum in $B \to X_u\ell\bar\nu$ [9] with the information on m_b and matrix elements of local operators known from $B \to X_c\ell\nu$ [10–12]. Given the theoretical input Γ^i_{mn} and M^j_{mn} computed in this paper, one needs to simply fit quadratic polynomials in the fit parameters c_n to the data. The experimental uncertainties and correlations in Γ^i and M^j and the theoretical uncertainties and correlations in Γ^i_{mn} and M^j_{mn} will translate to uncertainties of the coefficients c_n. In this approach, the uncertainty in the functional form of the F function is automatically and straightforwardly determined by the uncertainties of the coefficients $\{c_0, \ldots, c_N\}$, and the truncation error from approximating $\hat F(k)$ by $\hat F^{(N)}(k)$ discussed in Sec. IV B.

Finally, in Fig. 13 we combine our results to show the $B \to X_s\gamma$ spectrum $(d\Gamma_s/dE_\gamma)/[\Gamma_{0s}|C_7^{\rm incl}(0)|^2]$ in the B

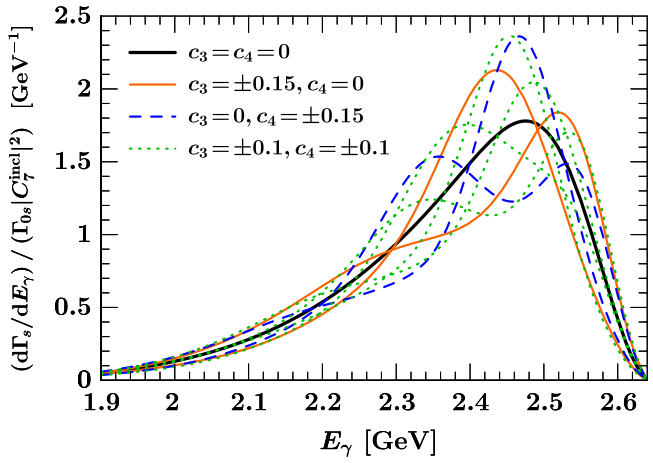

FIG. 13 (color online). The $B \to X_s\gamma$ photon spectrum in the B restframe using the nine shape function models shown in Fig. 10.

meson restframe. The results are shown using the short distance parameters m_b^{1S} and λ_1^i, and the nine shape function models plotted in Fig. 10, which have fixed zeroth, first, and second moments. The thick solid curve is our default model, $\hat{F}^{\rm mod}(k)$ in Eq. (34). In the current and future experimental analyses $m_B - 2E_\gamma \lesssim 2$ GeV. Our formalism has the virtue that we do not need to distinguish regions 1 and 2 in Eq. (3), i.e., it is simultaneously valid for both $m_B - 2E_\gamma^{\rm cut} \sim \Lambda_{\rm QCD}$ and $\gg \Lambda_{\rm QCD}$. The variation of the curves near maximal E_γ indicates that in the peak region the first few moments of the shape function are not sufficient to predict the spectrum. However, for $E_\gamma \lesssim 2.1$ GeV, the uncertainty in the prediction becomes significantly smaller, and the leading order shape function model uncertainty diminishes. The spectrum in this region is also affected by subleading shape functions and additional perturbative corrections not studied here. (Note that the measured spectrum is somewhat broadened by experimental effects.) We found the same conclusion using many other shape function models, constructed from different bases, and expect that this will also be substantiated by an actual experimental analysis in which the space of shape functions is explored by allowing for more components in our orthonormal basis and a simultaneous fit to all relevant data. This will have important implications for the $B \to X_s\gamma$ rate in the presence of an experimental cut, the extraction of $|V_{ub}|$ from inclusive semileptonic B decays, and the analysis of the inclusive $B \to X_s\ell^+\ell^-$ rate in the small q^2 region.

VI. CONCLUSIONS

In this paper, we introduced new methods for calculations relevant for inclusive B decays which involve the parton distribution function of the b quark in a B meson, called the shape function. On the theoretical side, our results allow for an improved description of the decay rates and a more reliable assessment of the uncertainties than earlier studies. On the experimental side, they are straightforward to implement and provide a transparent way to combine constraints on the shape and moments of the shape function, with controllable uncertainties.

The shape function is constrained by the measurements of the shape of the $B \to X_s\gamma$ photon energy spectrum [6–8] and the m_X spectrum in $B \to X_u\ell\bar{\nu}$ [9], and its moments are related to the b quark mass m_b and nonperturbative matrix elements of local operators in the OPE, which are constrained by fits to $B \to X_c\ell\bar{\nu}$ decay distributions [10–12].

The first key ingredient in our analysis is the new description of the shape function, given in Eq. (2) and discussed in detail in Sec. III, which is by construction consistent with the renormalization group evolution and the perturbative result for the tail of the shape function. It allows combining all experimental information from the shape of $B \to X_s\gamma$ and $B \to X_u\ell\bar{\nu}$ spectra, and m_b and λ_1 constrained by $B \to X_c\ell\bar{\nu}$ distributions. Any short distance scheme for the b quark mass and the kinetic energy matrix element can be implemented. We presented a simple formula for the differential rates which incorporates resummed perturbative corrections, with details of the derivation given in Appendixes A and B.

The second key ingredient in our analysis is the expansion of the F function, describing the nonperturbative part of the shape function, in a complete set of orthonormal functions in Sec. IV. This gives a new way to quantify uncertainties in the functional form of the shape function, which was previously not explored fully systematically. Choosing $Y(x)$ in Eq. (44) to coincide with any of the models used in the literature [28,33,34,45,46] gives an orthonormal basis for the shape function in which the first function is the model and corrections can be studied.

One should use renormalon-free short distance definitions for input parameters, such as the b quark mass, m_b, or the kinetic energy matrix element λ_1. We found that in our framework the kinetic scheme definition of $\lambda_1^{\rm kin}$ seems to oversubtract from the HQET definition of λ_1 in dimensional regularization, numerically similar to using the $\overline{\rm MS}$ mass for inclusive spectra. To solve this problem, in Appendix C we introduced a new short distance invisible scheme λ_1^i, which is renormalon-free and only differs from the usual definition starting at order α_s^2. While it does not improve the behavior of the perturbation series decisively, being almost invisible, at least it does not make it worse.

It should be emphasized that all developments presented in this paper are consistent with and incorporate all predictions that follow from QCD, without recourse to models or relying on any *ad hoc* assumptions. In fact, any method consistent with the factorization theorem and the OPE discussed in Sec. II can be cast in our framework.

Our results lead to the following strategy to determine $|V_{ub}|$ with optimal and reliable uncertainties:

(1) Fix a basis for the expansion of the F function by choosing a suitable $Y(x)$ and a value for λ.

(2) Do a combined fit to the binned $B \to X_s\gamma$ and/or $B \to X_u\ell\bar{\nu}$ spectra, and to the information on m_b and λ_1 from $B \to X_c\ell\bar{\nu}$ (and possibly higher moments) to extract the basis coefficients $\{c_0, \ldots, c_N\}$.
(3) Verify that the truncation error is small compared to other uncertainties.
(4) Use the values and covariance matrix of the extracted basis coefficients to make predictions with reliable uncertainties.

More details on the shape function fitting procedure, on extracting $|V_{ub}|$ from various $B \to X_u\ell\bar{\nu}$ differential decay distributions, and predictions for the $B \to X_s\gamma$ rate will be presented elsewhere.

ACKNOWLEDGMENTS

We thank Kerstin Tackmann for discussions and comments on the manuscript. Z. L. and I. S. thank the CERN Theory Group and the Aspen Center for Physics for hospitality while parts of this work were completed. F. T. thanks the particle physics group at Humboldt University Berlin for its hospitality during the final stages of this work. This work was supported in part by the Director, Office of Science, Offices of High Energy and Nuclear Physics of the U.S. Department of Energy under the Contract Nos. DE-AC02-05CH11231 and DE-FG02-94ER40818. I. S. was also supported in part by the DOE OJI program and by the Sloan Foundation.

APPENDIX A: PERTURBATIVE RESULTS

In this appendix we collect the known results for the hard functions $H_{u,s}(p_X^\pm, \mu_i)$ in Eq. (4), and derive an analytic result for the function $P(p^-, p_X^+, \mu_i)$ in Eq. (7), which includes perturbative corrections from the jet and soft functions as well as the shape function RGE. In Ref. [32] it was shown in the context of dijet production that the convolution form for the soft function analogous to Eq. (21) allows all factors associated with perturbative corrections and RGE to be evaluated analytically. Here we show that this is also true for inclusive B decays. Our calculation differs from Ref. [32] in that we develop a method that avoids using an imaginary part at intermediate steps. (An alternative analytic method that avoids the plus distributions by using moments was developed in Ref. [47].) Furthermore, with our basis for $\hat{F}(k)$, we show that the integrals over the basis function can be written in terms of hypergeometric functions.

We discuss fixed order results in Sec. A 1, the RGE in Sec. A 2, and the rate in short distance schemes in Sec. A 3. The definitions of the required plus distributions and many useful relations are collected in Appendix B.

1. Fixed order results

In Eqs. (4) and (6) the leading order hard function $H_s(p_X^+, \mu_i)$ for $B \to X_s\gamma$ is

$$H_s(p_X^+, \mu_i) = \frac{(m_B - p_X^+)^3}{m_b^3} |C_7^{\rm incl}(0)|^2 \times h_s(m_b, \mu_b) U_H(m_b, \mu_b, \mu_i), \quad \text{(A1)}$$

where the evolution factor $U_H(m_b, \mu_b, \mu_i)$ is given below in Eq. (A14), and has the boundary condition $U_H(m_b, \mu_b, \mu_b) = 1$. The Wilson coefficient $C_7^{\rm incl}$ in H_s contains the weak scale matching of the full theory onto the effective Hamiltonian from which the W and t are integrated out, and resums perturbative corrections between the weak scale and the scale $\mu \sim m_b$. It does not depend on μ_b and is defined by the split matching procedure in Ref. [4], which separates the perturbation series above and below the scale m_b. It can be written as [48]

$$C_7^{\rm incl}(0) = \mathcal{C}_7 + F_7(0) + G_7(0), \quad \text{(A2)}$$

with the central values $C_7^{\rm incl}(0) = -0.341 - 0.015i$ and $\mathcal{C}_7 = -0.261$. The Wilson coefficient $\mathcal{C}_7$ and the functions $F_7(q^2)$ and $G_7(q^2)$ are defined to be separately μ independent. Here, $\mathcal{C}_7$ contains the dependence on the $\overline{\rm MS}$ b quark mass and the Wilson coefficient $C_7(\mu)$ from the operator O_7 in the weak Hamiltonian,

$$\mathcal{C}_7 = C_7(u)\frac{\bar{m}_b(\mu)}{m_b} + C_i(\mu)\kappa_{i7} - \frac{\alpha_s(\mu)}{4\pi}\ln\frac{\mu}{m_b}\Big[\frac{8}{3}C_7(\mu)\frac{\bar{m}_b(u)}{m_b} - \frac{32}{9}C_8(\mu) + C_i(u)(\gamma_{ij}^{(0)}\kappa_{j7} + \gamma_{i7}^{(0)})\Big] + \mathcal{O}(\alpha_s^2). \quad \text{(A3)}$$

The Wilson coefficients $C_i(\mu)$, κ_{i7}, and the anomalous dimensions $\gamma_{ij}^{(0)}$ are with respect to the operator basis of Ref. [49] and are given explicitly in Ref. [48]. The function $F_7(q^2)$ contains perturbative corrections from other operators in the weak Hamiltonian, while $G_7(q^2)$ contains nonperturbative corrections from intermediate $c\bar{c}$ states. They are given in Eqs. (A5) and (A12) in Ref. [48].

The coefficient $h_s(m_b, \mu_b)$ in Eq. (A1) corresponds to the matching coefficient for the tensor current in SCET. At $\mathcal{O}(\alpha_s)$ it was computed in Ref. [50]. To determine the hard matching coefficient at $\mathcal{O}(\alpha_s^2)$ we take the two-loop computation of the $|C_7|^2$ terms in the $b \to s\gamma$ rate and spectrum from Refs. [51] and subtract the terms in the partonic two-loop spectrum in SCET coming from the jet and shape functions [given by $P(m_b, k, \mu_b)$ in Eq. (A30) below]. Because of the split matching, the μ_b dependence in $h_s(m_b, \mu_b)$ cancels entirely against the μ_b dependence in $U_H(m_b, \mu_b, \mu_i)$ in Eq. (A1), and does not depend on the μ dependence of the coefficients in the electroweak Hamiltonian. We obtain

$$h_s(m_b,\mu_b) = 1 - \frac{\alpha_s(\mu_b)}{\pi} C_F\left(\ln^2\frac{\mu_b}{m_b} + \frac{5}{2}\ln\frac{\mu_b}{m_b} + 3 + \frac{\pi^2}{24}\right) + \frac{\alpha_s^2(\mu_b)}{\pi^2} C_F\left\{\frac{1}{2}C_F\ln^4\frac{\mu_b}{m_b} + \left(\frac{5}{2}C_F - \frac{1}{6}\beta_0\right)\ln^3\frac{\mu_b}{m_b}\right.$$
$$+ \left[\left(\frac{49}{8} + \frac{\pi^2}{24}\right)C_F + \left(\frac{\pi^2}{12} - \frac{1}{3}\right)C_A - \frac{25}{24}\beta_0\right]\ln^2\frac{\mu_b}{m_b}$$
$$+ \left[\left(\frac{117}{16} + \frac{17\pi^2}{48} - 3\zeta_3\right)C_F + \left(\frac{\pi^2}{12} - \frac{29}{72} + \frac{11\zeta_3}{4}\right)C_A - \left(\frac{341}{144} + \frac{\pi^2}{12}\right)\beta_0\right]\ln\frac{\mu_b}{m_b} + 3.88611 C_F + 5.89413 C_A$$
$$\left. - \left(\frac{7859}{3456} + \frac{109\pi^2}{576} + \frac{13\zeta_3}{48}\right)\beta_0 + \frac{3563}{1296} - \frac{29\pi^2}{108} - \frac{\zeta_3}{6}\right\}. \tag{A4}$$

Our expressions here agree with the corresponding numerical results in Eq. (99) of Ref. [52]. Note that the inverse powers of m_b in Eqs. (A1), (A3), and (A5) below cancel the m_b^5 factors in $\Gamma_{0s,u}$ in Eq. (5), and any mass scheme can be used. The m_b appearing in $h_s(m_b,\mu_b)$ and $U_H(m_b,\mu_b,\mu_i)$ is defined in the pole scheme. Here, the pole mass renormalon ambiguity is less relevant, because m_b only appears as a reference scale for μ_b, so the effect of changing m_b is included in the variation of μ_b. For numerical calculations, we use $m_b = 4.7$ GeV.

The hard function $H_u(E_\ell, p_X^-, p_X^+, \mu_i)$ for $B \to X_u \ell\bar\nu$ in Eqs. (4) and (6) is given by

$$H_u(E_\ell, p_X^-, p_X^+, \mu_i) = \frac{24}{m_b^5}(m_B - p_X^+)(2E_\ell + p_X^- - m_B)\left\{(2m_B - p_X^+ - p_X^- - 2E_\ell)h_{u1}(m_b, p^-, \mu_b)\right.$$
$$\left. + (m_B - p_X^+ - 2E_\ell)\left[h_{u2}(m_b, p^-, \mu_b) + \frac{m_B - p_X^+}{p_X^- - p_X^+}h_{u3}(m_b, p^-, \mu_b)\right]\right\}U_H(p^-, \mu_b, \mu_i), \tag{A5}$$

where the $h_{ui}(m_b, p^-, \mu_b)$ correspond to the matching coefficients of the $V - A$ current in SCET. To order α_s [14,21,50]

$$h_{u1}(m_b, p^-, \mu_b) = 1 - \frac{\alpha_s(\mu_b)}{\pi}C_F\left[\ln^2\frac{\mu_b}{p^-} + \frac{5}{2}\ln\frac{\mu_b}{m_b} + \mathrm{Li}_2\left(1 - \frac{p^-}{m_b}\right) + \frac{3p^- - 2m_b}{2m_b - 2p^-}\ln\frac{p^-}{m_b} + \frac{\pi^2}{24} + 3\right],$$
$$h_{u2}(m_b, p^-, \mu_b) = \frac{\alpha_s(\mu_b)}{2\pi}C_F\frac{m_b}{m_b - p^-}\left(\frac{p^-}{m_b - p^-}\ln\frac{p^-}{m_b} + 1\right), \tag{A6}$$
$$h_{u3}(m_b, p^-, \mu_b) = \frac{\alpha_s(\mu_b)}{2\pi}C_F\frac{p^-}{m_b - p^-}\left(\frac{m_b - 2p^-}{m_b - p^-}\ln\frac{p^-}{m_b} - 1\right).$$

The corresponding two-loop results for H_u will be easy to implement once they become available. Finally, the evolution factor $U_H(p^-, \mu_b, \mu_i)$ in Eq. (A1) is identical for H_s and H_u, and is given below in Eq. (A14).

We now turn to the function $P(p^-, k, \mu_i)$ in Eq. (7). Changing variables $\omega \to \omega' + k - \omega$, we have

$$P(p^-, k, \mu_i) = \int d\omega U_S(k - \omega, \mu_i, \mu_\Lambda) \times \int d\omega' p^- J[p^-(\omega - \omega'), \mu_i] C_0(\omega', \mu_\Lambda). \tag{A7}$$

To incorporate the fixed order α_s corrections to the jet function $J(p^2, \mu_i)$, and the shape function kernel $C_0(\omega, \mu_\Lambda)$, we will first carry out the ω' convolution integral. The evolution factor $U_S(p_X^+, \mu_i, \mu_\Lambda)$, which sums logarithms between the scales μ_i and μ_Λ, and the integral over ω are discussed later.

To all orders in perturbation theory the jet function and shape function kernel can be written as

$$J(p^2, \mu_i) = \frac{1}{\mu_i^2}\sum_{n=-1}^{\infty} J_n[\alpha_s(\mu_i)]\mathcal{L}_n(p^2/\mu_i^2),$$
$$C_0(\omega, \mu_\Lambda) = \frac{1}{\mu_\Lambda}\sum_{n=-1}^{\infty} S_n[\alpha_s(\mu_\Lambda)]\mathcal{L}_n(\omega/\mu_\Lambda), \tag{A8}$$

where the $\mathcal{L}_n(x)$ are plus distributions defined in Eq. (B6) for $n \geq 0$ and in Eq. (B10) for $n = -1$, and the coefficients $J_n(\alpha_s)$ and $S_n(\alpha_s)$ have expansions in α_s. The jet function coefficients are known at one [21] and two loops [53], and are given by

$$
\begin{aligned}
J_{-1}(\alpha_s) &= 1 + \frac{\alpha_s}{\pi}\Big(\frac{7}{4} - \frac{\pi^2}{4}\Big)C_F + \frac{\alpha_s^2}{\pi^2}\Big[\Big(\frac{205}{128} - \frac{67\pi^2}{96} + \frac{7\pi^4}{120} - \frac{9\zeta_3}{8}\Big)C_F^2 + \Big(\frac{1417}{1728} - \frac{7\pi^2}{144} - \frac{17\pi^4}{2880} - \frac{9\zeta_3}{8}\Big)C_F C_A \\
&\quad + \Big(\frac{4057}{3456} - \frac{17\pi^4}{144} - \frac{\zeta_3}{12}\Big)C_F\beta_0\Big], \\
J_0(\alpha_s) &= -\frac{\alpha_s}{\pi}\frac{3}{4}C_F - \frac{\alpha_s^2}{\pi^2}\Big[\Big(\frac{45}{32} - \frac{7\pi^2}{16} + \frac{\zeta_3}{2}\Big)C_F^2 + \Big(\frac{73}{144} - \frac{5\zeta_3}{2}\Big)C_F C_A + \Big(\frac{247}{288} - \frac{\pi^2}{24}\Big)C_F\beta_0\Big], \\
J_1(\alpha_s) &= \frac{\alpha_s}{\pi}C_F + \frac{\alpha_s^2}{\pi^2}\Big[\Big(\frac{37}{16} - \frac{5\pi^2}{12}\Big)C_F^2 + \Big(\frac{1}{3} - \frac{\pi^2}{12}\Big)C_F C_A + \frac{29}{48}C_F\beta_0\Big], \\
J_2(\alpha_s) &= -\frac{\alpha_s^2}{\pi^2}\Big(\frac{9}{8}C_F^2 + \frac{1}{8}C_F\beta_0\Big), \\
J_3(\alpha_s) &= \frac{\alpha_s^2}{\pi^2}\frac{1}{2}C_F^2.
\end{aligned}
\tag{A9}
$$

The shape function coefficients to one [21] and two loops [54] are

$$
\begin{aligned}
S_{-1}(\alpha_s) &= 1 - \frac{\alpha_s}{\pi}\frac{\pi^2}{24}C_F - \frac{\alpha_s^2}{\pi^2}\Big[\Big(\frac{\pi^2}{12} + \frac{3\pi^4}{640} - 2\zeta_3\Big)C_F^2 + \Big(\frac{29}{108} + \frac{31\pi^2}{144} - \frac{67\pi^4}{2880} + \frac{9\zeta_3}{8}\Big)C_F C_A \\
&\quad + \Big(-\frac{1}{216} + \frac{5\pi^2}{576} - \frac{5\zeta_3}{48}\Big)C_F\beta_0\Big], \\
S_0(\alpha_s) &= -\frac{\alpha_s}{\pi}C_F + \frac{\alpha_s^2}{\pi^2}\Big[\Big(-\frac{7\pi^2}{24} + 4\zeta_3\Big)C_F^2 + \Big(\frac{11}{18} + \frac{\pi^2}{12} - \frac{9\zeta_3}{4}\Big)C_F C_A - \frac{1}{36}C_F\beta_0\Big], \\
S_1(\alpha_s) &= -\frac{\alpha_s}{\pi}2C_F + \frac{\alpha_s^2}{\pi^2}\Big[\Big(1 - \frac{7\pi^2}{12}\Big)C_F^2 + \Big(-\frac{2}{3} + \frac{\pi^2}{6}\Big)C_F C_A - \frac{1}{3}C_F\beta_0\Big], \\
S_2(\alpha_s) &= \frac{\alpha_s^2}{\pi^2}\Big(3C_F^2 + \frac{1}{2}C_F\beta_0\Big), \\
S_3(\alpha_s) &= \frac{\alpha_s^2}{\pi^2}2C_F^2.
\end{aligned}
\tag{A10}
$$

All other coefficients in J and C_0 start at higher orders in α_s.

To convolute $\mathcal{L}_n[p^-(\omega - \omega')/\mu_i^2]$ with $\mathcal{L}_m(\omega/\mu_\Lambda)$ we first rescale them to have the same dimensionless arguments. Using Eq. (B13), J and C_0 satisfy the rescaling identities

$$
\begin{aligned}
J(p^-\omega, \mu) &= \frac{1}{p - \xi}\sum_{n=-1}^{\infty} J_n\Big[\alpha_s(\mu), \frac{p^-\xi}{\mu^2}\Big]\mathcal{L}_n\Big(\frac{\omega}{\xi}\Big), \\
C_0(\omega, \mu) &= \frac{1}{\xi}\sum_{n=-1}^{\infty} S_n\Big[\alpha_s(\mu), \frac{\xi}{\mu}\Big]\mathcal{L}_n\Big(\frac{\omega}{\xi}\Big),
\end{aligned}
\tag{A11}
$$

where ξ is an arbitrary dimension-one parameter that we will choose at our convenience later on, and the rescaled coefficients are

$$
\begin{aligned}
J_{-1}(\alpha_s, x) &= J_{-1}(\alpha_s) + \sum_{n=0}^{\infty} J_n(\alpha_s)\frac{\ln^{n+1}x}{n+1}, \\
J_n(\alpha_s, x) &= \sum_{k=0}^{\infty}\frac{(n+k)!}{n!k!}J_{n+k}(\alpha_s)\ln^k x, \\
S_{-1}(\alpha_s, x) &= S_{-1}(\alpha_s) + \sum_{n=0}^{\infty} S_n(\alpha_s)\frac{\ln^{n+1}x}{n+1}, \\
S_n(\alpha_s, x) &= \sum_{k=0}^{\infty}\frac{(n+k)!}{n!k!}S_{n+k}(\alpha_s)\ln^k x.
\end{aligned}
\tag{A12}
$$

Using Eq. (A11), the convolution of J and C_0 in Eq. (A7) becomes

$$
\begin{aligned}
(J \otimes C_0)(\omega, \mu_i, \mu_\Lambda) &\equiv \int d\omega' p^- J[p^-(\omega - \omega'), \mu_i] C_0(\omega' \mu_\Lambda) \\
&= \sum_{m,n=-1}^{\infty} J_m\Big[\alpha_s(\mu_i), \frac{p^-\xi}{\mu_i^2}\Big] S_n\Big[\alpha_s(\mu_\Lambda), \frac{\xi}{\mu_\Lambda}\Big] \frac{1}{\xi} \int dx \mathcal{L}_m\Big(\frac{\omega}{\xi} - x\Big) \mathcal{L}_n(x) \\
&= \sum_{\ell=-1}^{\infty} \sum_{\substack{m,n\geq -1 \\ m+n+1\geq \ell}}^{\infty} V_\ell^{mn} J_m\Big[\alpha_s(\mu_i), \frac{p^-\xi}{\mu_i^2}\Big] S_n\Big[\alpha_s(\mu_\Lambda), \frac{\xi}{\mu_\Lambda}\Big] \frac{1}{\xi} \mathcal{L}_\ell\Big(\frac{\omega}{\xi}\Big).
\end{aligned} \tag{A13}
$$

In the last step we used Eq. (B16) to perform the x integral, yielding a sum of plus distributions, whose coefficients V_ℓ^{mn} are given in Eq. (B17).

2. Renormalization group evolution

Next, we summarize results for the renormalization group evolution, and then carry out the ω integral in Eq. (A7). The factor $U_H(p^-, \mu_b, \mu_i)$ which describes the evolution of the hard functions in Eqs. (A1) and (A5) between the hard scale μ_b, and the jet scale μ_i, is [50]

$$
U_H(p^-, \mu_b, \mu_i) = e^{K_H(\mu_i, \mu_b)} \Big(\frac{p^-}{\mu_b}\Big)^{\eta(\mu_i, \mu_b)}, \tag{A14}
$$

where definitions of $\eta(\mu_i, \mu_b)$ and $K_H(\mu_i, \mu_b)$ are given in Eq. (A17) below. The soft evolution factor $U_S(\omega, \mu_i, \mu_\Lambda)$ in Eq. (A7) sums logarithms between the jet scale μ_i, and soft scale μ_Λ. To all orders in perturbation theory it can be written as

$$
\begin{aligned}
U_S(\omega, \mu_i, \mu_\Lambda) &= e^{K_S(\mu_i, \mu_\Lambda)} \frac{e^{-\gamma_E \eta}}{\Gamma(\eta)} \frac{1}{\mu_\Lambda} \Big[\frac{\theta(\omega/\mu_\Lambda)}{(\omega/\mu_\Lambda)^{1-\eta}}\Big]_+^{\text{Ref. [32]}} \\
&= E_S(\xi, \mu_i, \mu_\Lambda) \frac{1}{\xi} \Big[\eta \mathcal{L}^\eta\Big(\frac{\omega}{\xi}\Big) + \mathcal{L}_{-1}\Big(\frac{\omega}{\xi}\Big)\Big],
\end{aligned} \tag{A15}
$$

where $\eta \equiv \eta(\mu_i, \mu_\Lambda)$, and we defined

$$
E_S(\xi, \mu_i, \mu_\Lambda) = e^{K_S(\mu_i, \mu_\Lambda)} \Big(\frac{\xi}{\mu_\Lambda}\Big)^\eta \frac{e^{-\gamma_E \eta}}{\Gamma(1+\eta)}. \tag{A16}
$$

To go from the first to the second line in Eq. (A15) we used Eqs. (B8) and (B12). An expression for $U_S(\omega, \mu_i, \mu_\Lambda)$ was first found in Ref. [13] and extended to all orders in Ref. [22]. The form with the plus distribution derived in Ref. [32] makes the formula valid without having to require $\mu_i > \mu_\Lambda$.

In Eqs. (A14) to (A16), $\eta(\mu, \mu_0)$ and $K_x(\mu, \mu_0)$ for $x = H$ or S are given to all orders by

$$
\begin{aligned}
\eta(\mu, \mu_0) &= 2 \int_{\alpha_s(\mu_0)}^{\alpha_s(\mu)} d\alpha_s \frac{\Gamma_{\text{cusp}}(\alpha_s)}{\beta(\alpha_s)}, \\
K_x(\mu, \mu_0) &= -2 \int_{\alpha_s(\mu_0)}^{\alpha_s(\mu)} d\alpha_s \Big[\frac{\Gamma_{\text{cusp}}(\alpha_s)}{\beta(\alpha_s)} \int_{\alpha_s(\mu_0)}^{\alpha_s} \frac{d\alpha_s'}{\beta(\alpha_s')} \\
&\quad + \frac{\gamma_x(\alpha_s)}{\beta(\alpha_s)}\Big].
\end{aligned} \tag{A17}
$$

Here, Γ_{cusp} is the universal cusp anomalous dimension. The only difference between K_H and K_S are the hard and soft anomalous dimensions $\gamma_x = \gamma_S$ or γ_H. Expanding the β function and anomalous dimensions as usual,

$$
\begin{aligned}
\beta(\alpha_s) &= -2\alpha_s \sum_{n=0}^{\infty} \beta_n \Big(\frac{\alpha_s}{4\pi}\Big)^{n+1}, \\
\Gamma_{\text{cusp}}(\alpha_s) &= \sum_{n=0}^{\infty} \Gamma_n \Big(\frac{\alpha_s}{4\pi}\Big)^{n+1}, \\
\gamma_x(\alpha_s) &= \sum_{n=0}^{\infty} \gamma_n^x \Big(\frac{\alpha_s}{4\pi}\Big)^{n+1},
\end{aligned} \tag{A18}
$$

the integrals in Eq. (A17) to NNLL are

$$
\begin{aligned}
\eta(\mu, \mu_0) &= -\frac{\Gamma_0}{\beta_0}\Big[\ln r + \frac{\alpha_s(\mu_0)}{4\pi}\Big(\frac{\Gamma_1}{\Gamma_0} - \frac{\beta_1}{\beta_0}\Big)(r-1) + \frac{\alpha_s^2(\mu_0)}{16\pi^2}\Big(\frac{\Gamma_2}{\Gamma_0} - \frac{\beta_1\Gamma_1}{\beta_0\Gamma_0} + \frac{\beta_1^2}{\beta_0^2} - \frac{\beta_2}{\beta_0}\Big)\frac{r^2-1}{2}\Big], \\
K_x(\mu, \mu_0) &= \frac{\Gamma_0}{2\beta_0^2}\Big\{\frac{4\pi}{\alpha_s(\mu_0)}\Big(1 - \frac{1}{r} - \ln r\Big) + \Big(\frac{\Gamma_1}{\Gamma_0} - \frac{\beta_1}{\beta_0}\Big)(1 - r + \ln r) + \frac{\beta_1}{2\beta_0}\ln^2 r + \frac{2\beta_0\gamma_0^x}{\Gamma_0}\ln r \\
&\quad + \frac{\alpha_s(\mu_0)}{4\pi}\Big[\Big(\frac{\beta_1^2}{\beta_0^2} - \frac{\beta_2}{\beta_0}\Big)\Big(\frac{1-r^2}{2} + \ln r\Big) + \Big(\frac{\beta_1\Gamma_1}{\beta_0\Gamma_0} - \frac{\beta_1^2}{\beta_0^2}\Big)(1 - r + r\ln r) - \Big(\frac{\Gamma_2}{\Gamma_0} - \frac{\beta_1\Gamma_1}{\beta_0\Gamma_0}\Big)\frac{(1-r)^2}{2} \\
&\quad + \frac{2\beta_0\gamma_0^x}{\Gamma_0}\Big(\frac{\gamma_1^x}{\gamma_0^x} - \frac{\beta_1}{\beta_0}\Big)(r-1)\Big]\Big\},
\end{aligned} \tag{A19}
$$

with $r = \alpha_s(\mu)/\alpha_s(\mu_0)$. When using $\eta(\mu, \mu_0)$ and $K_x(\mu, \mu_0)$ at LL, NLL, and NNLL according to our conventions in Eq. (25), we do not reexpand the results in Eqs. (A14) and (A16), but keep their full expressions everywhere. For the running coupling we always use the three-loop expression

$$\frac{1}{\alpha_s(\mu)} = \frac{X}{\alpha_s(\mu_0)} + \frac{\beta_1}{4\pi\beta_0}\ln X + \frac{\alpha_s(\mu_0)}{16\pi^2}\left[\frac{\beta_2}{\beta_0}\left(1-\frac{1}{X}\right) + \frac{\beta_1^2}{\beta_0^2}\left(\frac{\ln X}{X}+\frac{1}{X}-1\right)\right], \tag{A20}$$

where $X \equiv 1 + \alpha_s(\mu_0)\beta_0 \ln(\mu/\mu_0)/(2\pi)$, and we evolve to lower scales using the reference value $\alpha_s(\mu_0 = 4.7\ \text{GeV}) = 0.2155$ as in Table I with $n_f = 4$. Up to three-loop order, the coefficients of the β function in the $\overline{\text{MS}}$ scheme are

$$\begin{aligned}
\beta_0 &= \frac{11}{3}C_A - \frac{2}{3}n_f,\\
\beta_1 &= \frac{34}{3}C_A^2 - \frac{10}{3}C_A n_f - 2C_F n_f,\\
\beta_2 &= \frac{2857}{54}C_A^3 + \left(C_F^2 - \frac{205}{18}C_F C_A - \frac{1415}{54}C_A^2\right)n_f + \left(\frac{11}{9}C_F + \frac{79}{54}C_A\right)n_f^2.
\end{aligned} \tag{A21}$$

The cusp [55,56], soft [57,58], and hard anomalous dimension coefficients are

$$\begin{aligned}
\Gamma_0 &= 4C_F,\\
\Gamma_1 &= \left(\frac{268}{9} - \frac{4\pi^2}{3}\right)C_F C_A - \frac{40}{9}C_F n_f,\\
\Gamma_2 &= \left(\frac{490}{3} - \frac{536\pi^2}{27} + \frac{44\pi^4}{45} + \frac{88\zeta_3}{3}\right)C_F C_A^2 + \left(\frac{80\pi^2}{27} - \frac{836}{27} - \frac{112\zeta_3}{3}\right)C_F C_A n_f + \left(32\zeta_3 - \frac{110}{3}\right)C_F^2 n_f - \frac{16}{27}C_F n_f^2,\\
\gamma_0^S &= -2C_F,\\
\gamma_1^S &= \left(\frac{110}{27} + \frac{\pi^2}{18} - 18\zeta_3\right)C_F C_A + \left(\frac{4}{27} + \frac{\pi^2}{9}\right)C_F n_f,\\
\gamma_0^H &= 5C_F,\\
\gamma_1^H &= \left(\frac{3}{2} - 2\pi^2 + 24\zeta_3\right)C_F^2 - \left(\frac{125}{27} + \frac{\pi^2}{3}\right)C_F n_f + \left(\frac{1549}{54} + \frac{7\pi^2}{6} - 22\zeta_3\right)C_F C_A.
\end{aligned} \tag{A22}$$

To determine γ_1^H we used $\gamma_1^H = -\gamma_1^J - \gamma_1^S$, which follows from the μ independence of $d\Gamma_s/d E_\gamma$. We use the two-loop computation of γ_1^J in Ref. [53].

The evolution of the shape function kernel $C_0(\omega, \mu)$ from μ_Λ to μ_i can be written as the sum of a finite number of terms,

$$\begin{aligned}
C_0(\omega, \mu_i) &= \int d\omega' U_S(\omega - \omega', \mu, \mu_\Lambda) C_0(\omega', \mu_\Lambda)\\
&= E_S(\xi, \mu_i, \mu_\Lambda)\sum_{n=-1}^{\infty} S_n\left[\alpha_s(\mu_\Lambda), \frac{\xi}{\mu_\Lambda}\right] \times \frac{1}{\xi}\left[\eta\int dx\, \mathcal{L}^\eta\left(\frac{\omega}{\xi} - x\right)\mathcal{L}_n(x) + \mathcal{L}_n\left(\frac{\omega}{\xi}\right)\right]\\
&= E_S(\xi, \mu_i, \mu_\Lambda)\sum_{n=-1}^{\infty}\sum_{\ell=-1}^{n+1} V_\ell^n(\eta) \times S_n\left[\alpha_s(\mu_\Lambda), \frac{\xi}{\mu_\Lambda}\right]\frac{1}{\xi}\mathcal{L}_\ell^\eta\left(\frac{\omega}{\xi}\right).
\end{aligned} \tag{A23}$$

In the last step, we used Eq. (B16) to perform the x integral. The coefficients of the resulting plus distributions $V_\ell^n(\eta)$ are defined in Eq. (B17). If $C_0(\omega, \mu)$ is known to $\mathcal{O}(\alpha_s^k)$ accuracy, then the terms contributing in Eq. (A23) are bounded by $n \le 2k - 1$. To obtain the shape function evolved up to μ_i, $S(\omega, \mu_i)$, we combine Eq. (21) with (A23) taking for convenience $\xi = \omega$ and changing the integration variable to z via $k = \omega(1 - z)$. This gives the result for $S(\omega, \mu_i)$ that is quoted in Eq. (24) in the text.

Returning to $P(p^-, k, \mu_i)$ in Eq. (A7), to perform the ω integral we can now apply the same steps as in Eq. (A23) to compute the convolution of $U_S(\omega, \mu_i, \mu_\Lambda)$ with the result of Eq. (A13). This yields

$$P(p^-, k, \mu_i) = \sum_{j=-1}^{\infty} P_j(p^-, \xi, \mu_i, \mu_\Lambda)\frac{1}{\xi}\mathcal{L}_j^\eta\left(\frac{k}{\xi}\right), \tag{A24}$$

where $\eta = \eta(\mu_i, \mu_\Lambda)$, and the coefficients are

$$\begin{aligned}
&P_j(p^-, \xi, \mu_i, \mu_\Lambda)\\
&= E_S(\xi, \mu_i, \mu_\Lambda)\sum_{\substack{m,n\ge -1\\ m+n+2\ge j}}^{\infty}\left\{\sum_{\substack{\ell\ge -1\\ \ell\ge j-1}}^{m+n+1} V_\ell^{mn} V_j^\ell(\eta) \times J_m\left[\alpha_s(\mu_i), \frac{p^-\xi}{\mu_i^2}\right]S_n\left[\alpha_s(\mu_\Lambda), \frac{\xi}{\mu_\Lambda}\right]\right\},
\end{aligned} \tag{A25}$$

with $V_j^\ell(\eta)$ and V_ℓ^{mn} given in Eqs. (B17) and (B18). The jet and shape function coefficients J_m and S_n have perturbative expansions in $\alpha_s(\mu_i)$ and $\alpha_s(\mu_\Lambda)$, respectively, given by Eqs. (A9) and (A10) together with Eq. (A11). To $\mathcal{O}(\alpha_s)$ we have $m, n \le 1$, so dropping cross terms of $\mathcal{O}(\alpha_s^2)$ and higher, we need $-1 \le \ell \le 1$ and $-1 \le j \le 2$. To $\mathcal{O}(\alpha_s^2)$, we have $m, n \le 3$, and we need cross terms between J_m and S_n up to $-1 \le \ell \le 3$ and $-1 \le j \le 4$.

The final step now is to compute the convolution of $P(p^-, k, \mu_i)$ with some function $F(k)$,

$$\begin{aligned}
&\int dk P(p^-, k, \mu_i) F(p_X^+ - k)\\
&= \sum_{j=-1}^{\infty} P_j(p^-, p_X^+, \mu_i, \mu_\Lambda)\int_0^1 dz\, \mathcal{L}_j^\eta(z) F[p_X^+(1 - z)].
\end{aligned} \tag{A26}$$

In both Eqs. (24) and (A26) the remaining integral that needs to be performed is $\mathcal{L}_j^\eta(z)$ with $F[\omega(1-z)]$. For $j \geq 0$ it is convenient to simplify this integral to

$$\begin{aligned}&\int_0^1 dz \mathcal{L}_j^\eta(z) F[\omega(1-z)] \\ &= \int_0^1 dz \frac{\ln^j z}{z^{1-\eta}} \{F[\omega(1-z)] - F(\omega)\} \\ &= \frac{1}{\eta^{1+j}} \int_0^1 dt \ln^j t \{F[\omega(1-t^{1/\eta})] - F(\omega)\},\end{aligned} \tag{A27}$$

where the second line is valid for $\eta > -1$, but the last line only for $\eta > 0$. For $j = -1$ the integral is trivial since $\mathcal{L}_{-1}^\eta(z) = \delta(z)$. Our basis for $F(k)$ involves a series of terms of the form

$$F(k) = \sum_{r,s} C_{rs} \left(\frac{k}{\lambda}\right)^r \exp\left(-s\frac{k}{\lambda}\right), \tag{A28}$$

where r and s are integers. For each term in the series the integral in Eq. (A27) can be performed analytically using

$$\begin{aligned}&\int_0^1 dz [(1-z)^\ell e^{bz} - 1] z^{a+\eta-1} \\ &= -\frac{1}{a+\eta} + \frac{\Gamma(a+\eta)\Gamma(1+\ell)}{\Gamma(1+a+\eta+\ell)} \\ &\quad \times {}_1F_1(a+\eta, 1+a+\eta+\ell, b).\end{aligned} \tag{A29}$$

By taking derivatives of this result with respect to a one can obtain the integral with $(\ln z)^j$ on the left-hand side. In practice, we find that the numerical integration of Eq. (A27) is sufficiently fast that using Eq. (A29) is unnecessary.

Finally, we comment on a special case of the above results that was used to carry out the $B \to X_s\gamma$ matching computation to derive Eq. (A4). Here we used the SCET computation of the decay rate with $\mu_b = \mu_i = \mu_\Lambda = m_b$ and $\eta = 0$, which depends on $P(m_b, p_X^+, m_b)$. For this special case, the choice $\xi = m_b$ is convenient and Eqs. (A24) and (A25) then reduce to

$$\begin{aligned}P(m_b, p_X^+, m_b) &= \sum_{j=-1}^\infty P_j(m_b, m_b, m_b, m_b) \frac{1}{m_b} \mathcal{L}_j\left(\frac{p_X^+}{m_b}\right), \\ P_j(m_b, m_b, m_b, m_b) &= \sum_{\substack{m,n\geq -1 \\ m+n+2\geq j}}^\infty V_j^{mn} J_m[\alpha_s(m_b)] S_n[\alpha_s(m_b)].\end{aligned} \tag{A30}$$

Thus $P_j(m_b, m_b, m_b, m_b)$ is the coefficient of the plus distribution or δ distribution $\mathcal{L}_j$ in the fixed-order computation evaluated at $\mu = m_b$.

3. Changing to short distance schemes

To change the scheme from the pole scheme to a short distance scheme, we define a perturbative function $\hat{P}$ as in Eq. (7), but with C_0 replaced by $\hat{C}_0$, and in the differential spectrum P and F are replaced by $\hat{P}$ and $\hat{F}$. Displaying only the integration variables,

$$d\Gamma_q = \Gamma_{0q} H_q \int dk \hat{P}(k) \hat{F}(p_X^+ - k), \tag{A31}$$

with

$$\begin{aligned}\hat{P}(k) &= \int d\omega U_S(k-\omega) \int d\omega' J(\omega-\omega') \hat{C}_0(\omega') \\ &= \left\{1 + \delta m_b \frac{d}{dk} + \left[\frac{(\delta m_b)^2}{2} - \frac{\delta\lambda_1}{6}\right]\frac{d^2}{dk^2}\right\} P(k),\end{aligned} \tag{A32}$$

and δm_b and $\delta\lambda_1$ defined in Eq. (28). This result has exactly the same form as Eq. (33), which relates $\hat{C}_0(\omega)$ and $C_0(\omega)$, so the analysis we carry out below also holds for determining $\hat{P}(k)$ and $\hat{C}_0(\omega)$. To be definite, we use $\hat{P}(k)$ below. The results for $\hat{C}_0(\omega)$ are obtained by substituting $P(k) \to C_0(\omega)$.

To ensure the proper cancellation of renormalon ambiguities, the perturbative series in δm_b, $\delta\lambda_1$, and $P(k)$ have to be reexpanded to the desired order. Denoting

$$\begin{aligned}P(k) &= \sum_{n=0}^\infty \epsilon^n P^{(n)}(k), \\ \delta m_b &= \sum_{n=1}^\infty \epsilon^n \delta m_b^{(n)}(\mu_\Lambda), \\ \delta\lambda_1 &= \sum_{n=1}^\infty \epsilon^n \delta\lambda_1^{(n)}(\mu_\Lambda),\end{aligned} \tag{A33}$$

where the dummy variable $\epsilon = 1$ counts the order in the perturbative expansion. As indicated, the scale for α_s in δm_b and $\delta\lambda_1$ must be set to μ_Λ to ensure that renormalons cancel. To illustrate this, the μ_Λ variation in Fig. 3 yields the numbers $0.74, 0.76, 0.72\ \text{GeV}^{-1}$ for $S(\omega = 0.5\ \text{GeV}, \mu)$ at NNLL. However, holding μ_Λ in δm_b fixed at the central value the result becomes $0.81, 0.76, 0.68\ \text{GeV}^{-1}$, with a much larger scale dependence.

For $P(k)$, we count both $\alpha_s(\mu_i) \sim \epsilon$ and $\alpha_s(\mu_\Lambda) \sim \epsilon$ in S_n and J_m, i.e., we expand the cross terms between J_m and S_n. Note that we do not expand the cross terms in the product of H_q and $\hat{P}$ in Eq. (A31). Then, to $\mathcal{O}(\epsilon^2)$|

$$\begin{aligned}\hat{P}(k) &= \epsilon^0 P^{(0)}(k) + \epsilon^1 P^{(1)}(k) + \epsilon^2 P^{(2)}(k) \\ &\quad + \left[\delta m_b^{(1)} \frac{d}{dk} - \frac{\delta\lambda_1^{(1)}}{6}\frac{d^2}{dk^2}\right][\epsilon P^{(0)}(k) + \epsilon^2 P^{(1)}(k)] \\ &\quad + \epsilon^2 \left\{\delta m_b^{(2)} \frac{d}{dk} + \left[\frac{(\delta m_b^{(1)})^2}{2} - \frac{\delta\lambda_1^{(2)}}{6}\right]\frac{d^2}{dk^2}\right\} P^{(0)}(k),\end{aligned} \tag{A34}$$

and integrating by parts we can move the derivatives to act on $\hat{F}(k)$,

$$\int dk\hat{P}(k)\hat{F}(p_X^+ - k) = \int dk[P^{(0)}(k) + \epsilon P^{(1)}(k) + \epsilon^2 P^{(2)}(k)]\hat{F}(p_X^+ - k) + [(\epsilon\delta m_b^{(1)} + \epsilon^2\delta m_b^{(2)})P^{(0)}(k) + \epsilon^2\delta m_b^{(1)}P^{(1)}(k)]\hat{F}'(p_X^+ - k) + \left\{\left[-\epsilon\frac{\delta\lambda_1^{(1)}}{6} + \epsilon^2\frac{3(\delta m_b^{(1)})^2 - \delta\lambda_1^{(2)}}{6}\right]P^{(0)}(k) - \epsilon^2\frac{\delta\lambda_1^{(1)}}{6}P^{(1)}(k)\right\}\hat{F}''(p_X^+ - k). \quad \text{(A35)}$$

For m_b, we mostly use the $1S$ scheme [30], in which

$$\delta m_b^{(1S,1)} = R^{1S}\frac{\alpha_s(u)C_F}{8}, \qquad \delta m_b^{(1S,2)} = R^{1S}\frac{\alpha_s^2(\mu)C_F}{8\pi}\left[\left(\ln\frac{\mu}{R^{1S}} + \frac{11}{6}\right)\beta_0 - \frac{4}{3}C_A\right], \quad \text{(A36)}$$

where $R^{1S} = m_b^{1S}\alpha_s(\mu)C_F$. For λ_1, we use our invisible scheme, in which

$$\delta\lambda_1^{(\mathrm{i},1)} = 0, \qquad \delta\lambda_1^{(\mathrm{i},2)} = R^2\frac{\alpha_s^2(\mu)}{\pi^2}\frac{C_F C_A}{4}\left(\frac{\pi^2}{3} - 1\right). \quad \text{(A37)}$$

By default we take $R = 1$ GeV.

We also list the corresponding expressions in the kinetic scheme [31], defining $\lambda_1^{\mathrm{kin}} = -\mu_\pi^2$ and using R for the momentum cutoff,

$$\delta\lambda_1^{(\mathrm{kin},1)} = R^2\frac{\alpha_s(\mu)}{\pi}C_F, \qquad \delta\lambda_1^{(\mathrm{kin},2)} = R^2\frac{\alpha_s^2(\mu)}{\pi^2}\frac{C_F}{2}\left[\left(\ln\frac{\mu}{2R} + \frac{13}{6}\right)\beta_0 + \left(\frac{13}{6} - \frac{\pi^2}{3}\right)C_A\right],$$
$$\delta m_b^{(\mathrm{kin},1)} = R\frac{\alpha_s(\mu)}{\pi}\frac{4}{3}C_F + \frac{\delta\lambda_1^{(\mathrm{kin},1)}}{2m_b}, \qquad \delta m_b^{(\mathrm{kin},2)} = R\frac{\alpha_s^2(\mu)}{\pi^2}\frac{2}{3}C_F\left[\left(\ln\frac{\mu}{2R} + \frac{8}{3}\right)\beta_0 + \left(\frac{13}{6} - \frac{\pi^2}{3}\right)C_A\right] + \frac{\delta\lambda_1^{(\mathrm{kin},2)}}{2m_b}. \quad \text{(A38)}$$

By default in the kinetic scheme $R = 1$ GeV.

APPENDIX B: PLUS DISTRIBUTIONS AND CONVOLUTIONS

We define a general plus distribution for some function $q(x)$, which is less singular than $1/x^2$ as $x \to 0$, as

$$[q(x)]_+^{[x_0]} \equiv [\theta(x)q(x)]_+^{[x_0]} = \lim_{\epsilon\to 0}\frac{d}{dx}[\theta(x-\epsilon)Q(x,x_0)] = \lim_{\epsilon\to 0}[\theta(x-\epsilon)q(x) + \delta(x-\epsilon)Q(x,x_0)], \quad \text{(B1)}$$

with

$$Q(x,x_0) = \int_{x_0}^x dx' q(x'). \quad \text{(B2)}$$

Since $Q(x_0,x_0) = 0$, the point x_0 should be thought of as a boundary condition for the plus distribution. Integrating against a test function $f(x)$, we have

$$\int_{-\infty}^{x_{\max}} dx[\theta(x)q(x)]_+^{[x_0]}f(x) = \int_0^{x_{\max}} dx q(x)[f(x) - f(0)] + f(0)Q(x_{\max},x_0). \quad \text{(B3)}$$

Taking $f(x) = 1$ in Eq. (B3) one sees that the integral of the plus distribution vanishes only when integrated over a range with $x_{\max} = x_0$. Plus distributions with different boundary conditions are related to each other by

$$[\theta(x)q(x)]_+^{[x_0]} = [\theta(x)q(x)]_+^{[x_1]} + \delta(x)Q(x_1,x_0). \quad \text{(B4)}$$

We will almost exclusively use the boundary condition $x_0 = 1$, and will drop the superscript $[x_0]$ on the plus distributions when this default choice is used.

Taking the special case $q(x) = 1/x^{1-a}$ with $a > -1$, we define

$$\mathcal{L}^a(x) = \left[\frac{\theta(x)}{x^{1-a}}\right]_+ = \lim_{\epsilon\to 0}\frac{d}{dx}\left[\theta(x-\epsilon)\frac{x^a - 1}{a}\right]. \quad \text{(B5)}$$

With our boundary condition, $\mathcal{L}^a(x)$ for $a = 0$ reduces to the standard definition of $[\theta(x)/x]_+$. For $q(x) = \ln^n x/x$ with integer $n \geq 0$ we define

$$\mathcal{L}_n(x) = \left[\frac{\theta(x)\ln^n x}{x}\right]_+ = \lim_{\epsilon\to 0}\frac{d}{dx}\left[\theta(x-\epsilon)\frac{\ln^{n+1}x}{n+1}\right]. \quad \text{(B6)}$$

Since both $\mathcal{L}^a(x)$ and $\mathcal{L}_n(x)$ are defined with the same boundary condition $x_0 = 1$, they are related by

$$\mathcal{L}_n(x) = \frac{d^n}{da^n}\mathcal{L}^a(x)|_{a=0}. \quad \text{(B7)}$$

This makes it easy to derive identities involving $\mathcal{L}_n(x)$ from identities involving $\mathcal{L}^a(x)$ by taking derivatives with respect to a.

The definitions in Eqs. (B5) and (B6) can be contrasted with those in Ref. [32], where the same boundary condition

$x_0 = 1$ is used for $[\theta(x)\ln^n x/x]_+ = \mathcal{L}_n(x)$, but $x_0 = \infty$ and $x_0 = 0$ are used for $[\theta(x)/x^{1-a}]_+$ with $a < 0$ and $a > 0$, respectively. This is the form appearing in the soft evolution factor Eq. (A16), where it comes multiplied by a factor of a, so the limit for $a \to 0$ exists. Using Eq. (B4) to convert to our definitions, we have

$$\left[\frac{\theta(x)}{x^{1-a}}\right]_+ \overset{\text{Ref. [32]}}{=} \mathcal{L}^a(x) + \frac{1}{a}\delta(x). \tag{B8}$$

Finally, we define the "mixed" distribution

$$\mathcal{L}^a_n(x) = \left[\frac{\theta(x)\ln^n x}{x^{1-a}}\right]_+ = \frac{d^n}{db^n}\mathcal{L}^{a+b}(x)|_{b=0}, \tag{B9}$$

which satisfies $\mathcal{L}^0_n(x) \equiv \mathcal{L}_n(x)$ and $\mathcal{L}^a_0(x) \equiv \mathcal{L}^a(x)$. For convenience we also define

$$\mathcal{L}_{-1}(x) \equiv \mathcal{L}^a_{-1}(x) \equiv \delta(x). \tag{B10}$$

The following identities are useful

$$\begin{aligned}
\mathcal{L}_{m+n}(x) &= \frac{d^m}{da^m}\mathcal{L}^a_n(x)\bigg|_{a=0},\\
\mathcal{L}_{m+n+1}(x) &= (m+1)\frac{d^m}{da^m}\frac{\mathcal{L}^a_n(x) - \mathcal{L}_n(x)}{a}\bigg|_{a=0},\\
\mathcal{L}^a_{m+1}(x) &= (m+1)\frac{d^m}{db^m}\frac{\mathcal{L}^{a+b}(x) - \mathcal{L}^a(x)}{b}\bigg|_{b=0}.
\end{aligned} \tag{B11}$$

The $\mathcal{L}^a(x)$ satisfies the rescaling identity (for $\lambda > 0$)

$$\begin{aligned}
\lambda\mathcal{L}^a(\lambda x) &= \lim_{\epsilon\to 0}\frac{d}{dx}\left[\theta(x-\epsilon)\frac{(\lambda x)^a - 1}{a}\right]\\
&= \lambda^a\mathcal{L}^a(x) + \frac{\lambda^a - 1}{a}\delta(x),
\end{aligned} \tag{B12}$$

from which we can obtain the rescaling identity for $\mathcal{L}_n(x)$,

$$\begin{aligned}
\lambda\mathcal{L}_n(\lambda x) &= \frac{d^n}{da^n}\lambda^a\mathcal{L}^a(x)\bigg|_{a=0} + \frac{\ln^{n+1}\lambda}{n+1}\delta(x)\\
&= \sum_{k=0}^{n}\binom{n}{k}\ln^k\lambda\,\mathcal{L}_{n-k}(x) + \frac{\ln^{n+1}\lambda}{n+1}\delta(x).
\end{aligned} \tag{B13}$$

This agrees with the result in Eq. (C3) of Ref. [32]. We will also need convolutions of two plus distributions,

$$\begin{aligned}
\int dy\,\mathcal{L}^a(x-y)\mathcal{L}^b(y) &= \lim_{\epsilon\to 0}\frac{d}{dx}\left\{\theta(x-\epsilon)\left[\frac{x^{a+b}}{a+b}V(a,b) + \frac{x^a-1}{a}\frac{x^b-1}{b}\right]\right\}\\
&= \left(\mathcal{L}^{a+b}(x) + \frac{\delta(x)}{a+b}\right)V(a,b) + \left(\frac{1}{a}+\frac{1}{b}\right)\mathcal{L}^{a+b}(x) - \frac{1}{b}\mathcal{L}^a(x) - \frac{1}{a}\mathcal{L}^b(x).
\end{aligned} \tag{B14}$$

In the second step we used the definition in Eq. (B5). Here $V(a,b)$ is defined by

$$V(a,b) = \frac{\Gamma(a)\Gamma(b)}{\Gamma(a+b)} - \frac{1}{a} - \frac{1}{b}, \tag{B15}$$

which satisfies $V(0,0) = 0$. Taking derivatives with respect to a and b we can get the corresponding formulas for convolutions involving $\mathcal{L}_n$,

$$\begin{aligned}
\int dy\,\mathcal{L}^a(x-y)\mathcal{L}_n(y) &= \frac{d^n}{db^n}\left(\mathcal{L}^{a+b}(x) + \frac{\delta(x)}{a+b}\right)V(a,b)\bigg|_{b=0} + \frac{\mathcal{L}^a_{n+1}(x)}{n+1} + \frac{\mathcal{L}^a_n(x) - \mathcal{L}_n(x)}{a}\\
&\equiv \frac{1}{a}\sum_{k=-1}^{n+1}V^n_k(a)\mathcal{L}^a_k(x) - \frac{1}{a}\mathcal{L}_n(x),\\
\int dy\,\mathcal{L}_m(x-y)\mathcal{L}_n(y) &= \frac{d^m}{da^m}\frac{d^n}{db^n}\left(\mathcal{L}^{a+b}(x) + \frac{\delta(x)}{a+b}\right)V(a,b)\bigg|_{a=b=0} + \left(\frac{1}{m+1}+\frac{1}{n+1}\right)\mathcal{L}_{m+n+1}(x)\\
&\equiv \sum_{k=-1}^{m+n+1}V^{mn}_k\mathcal{L}_k(x).
\end{aligned} \tag{B16}$$

The result in the second line of Eq. (B16) reproduces a result given in Eq. (B6) of Ref. [59]. The coefficients $V^n_k(a)$ and V^{mn}_k are related to the Taylor series expansion of $V(a,b)$ around $a = 0$ and $a = b = 0$. The nonzero terms for $n \geq 0$ are

$$V^n_k(a) = \begin{cases} a\frac{d^n}{db^n}\frac{V(a,b)}{a+b}\Big|_{b=0}, & k = -1,\\ a\binom{n}{k}\frac{d^{n-k}}{db^{n-k}}V(a,b)\Big|_{b=0} + \delta_{kn}, & 0 \leq k \leq n,\\ \frac{a}{n+1}, & k = n+1. \end{cases} \tag{B17}$$

The term δ_{kn} in $V_k^n(a)$ and the last coefficient $V_{n+1}^n(a)$ arise from the boundary terms in the convolution integral. The V_k^{mn} are symmetric in m and n, and the nonzero terms for $m, n \geq 0$ are

$$V_k^{mn} = \begin{cases} \left.\frac{d^m}{da^m}\frac{d^n}{db^n}\frac{V(a,b)}{a+b}\right|_{a=b=0}, & k=-1, \\ \left.\sum_{p=0}^{m}\sum_{q=0}^{n}\delta_{p+q,k}\binom{m}{p}\binom{n}{q}\frac{d^{m-p}}{da^{m-p}}\frac{d^{n-q}}{db^{n-q}}V(a,b)\right|_{a=b=0}, & 0\leq k\leq m+n, \\ \frac{1}{m+1}+\frac{1}{n+1}, & k=m+n+1. \end{cases} \tag{B18}$$

The last coefficient V_{m+n+1}^{mn} again contains the boundary term. Using Eq. (B10) we can extend the results in Eq. (B16) to include the cases $n=-1$ or $m=-1$. The relevant coefficients are

$$V_{-1}^{-1}(a)=1, \qquad V_0^{-1}(a)=a, \qquad V_{k\geq 1}^{-1}(a)=0, \qquad V_k^{-1,n}=V_k^{n,-1}=\delta_{nk}. \tag{B19}$$

APPENDIX C: THE INVISIBLE SCHEME FOR λ_1

In this appendix we define a new scheme for λ_1, which we call the invisible scheme. It is a short distance scheme, free of the $u=1$ renormalon ambiguity, and it only deviates from the standard HQET definition of λ_1 at $\mathcal{O}(\alpha_s^2)$. Since the renormalon in λ_1 depends on the regularization scheme and, in particular, its symmetries [60,61], it is desirable to define λ_1 using a scheme which has the same symmetries as the multiloop dimensional regularization calculations of its coefficient function.

For a general ultraviolet (UV) regulator $\Lambda_{\rm UV}$, the bare kinetic energy operator is

$$[\bar b_v (iD_\perp)^2 b_v]_{\rm bare} = Z_1 \bar b_v b_v + Z_{\rm kin}\bar b_v (iD_\perp)^2 b_v + \cdots, \tag{C1}$$

where $Z_I \propto \Lambda_{\rm UV}^2$ and the ellipses denote higher dimension operators whose coefficients vanish as $\Lambda_{\rm UV}\to\infty$. Usually the kinetic energy matrix element in HQET is defined by

$$\lambda_1 = \langle B|\bar b_v (iD_\perp)^2 b_v|B\rangle, \tag{C2}$$

where UV divergences are regulated in dimensional regularization (we follow our convention of using full B states even if this is not always the practice in HQET). In that case, power divergences do not appear, so in Eq. (C1) $Z_1 = 0$. Furthermore, since this scheme respects reparametrization invariance [62], $Z_{\rm kin}=1$ and λ_1 is μ independent. Nonperturbatively λ_1 can still be sensitive to the quadratic UV divergence of Z_1 through a $u=1$ renormalon. The presence of this renormalon implies that there is an $\mathcal{O}(\Lambda_{\rm QCD}^2)$ ambiguity in the definition in Eq. (C2). In observables like a decay rate this λ_1 ambiguity cancels against a corresponding infrared renormalon ambiguity in the large-order behavior of the perturbation series in the leading order Wilson coefficients [63].

We use the notation $\hat\lambda_1$ for a generic short distance definition, which does not suffer from the renormalon ambiguity. Any $\hat\lambda_1$ can be related to λ_1 by a perturbative series $\delta\lambda_1 \sim \alpha_s + \alpha_s^2 + \cdots$, where $\hat\lambda_1 = \lambda_1 - \delta\lambda_1$. For the kinetic scheme the $u=1$ renormalon ambiguity is avoided by defining $\lambda_1^{\rm kin}$ using the second moment of a time-ordered product of currents with an explicit hard cutoff regulator μ_f [64]. Here Z_1 and $\delta\lambda_1 \propto \mu_f^2\alpha_s$. Since the kinetic energy operator mixes into $\bar b_v b_v$, it modifies the perturbation series multiplying $\bar b_v b_v$, and it is believed that this removes the corresponding $u=1$ infrared renormalon in the Wilson coefficients. In Ref. [14], a "shape function" scheme for λ_1 was introduced based on the second moment of $S(\omega,\mu)$ with a cutoff, which also has $\delta\lambda_1 \propto \mu_f^2\alpha_s$. A potential problem with these schemes is that they resolve an issue with the large-order behavior of perturbation theory by introducing a series that starts with a term $\delta\lambda_1 \sim \alpha_s$. While the inclusion of an $\mathcal{O}(\alpha_s)$ term is known to provide good numerical stability when removing the

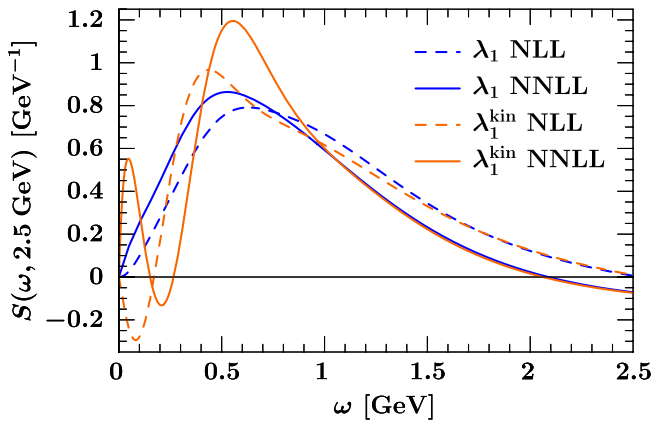

FIG. 14 (color online). Effect of the short distance subtractions $\delta\lambda_1^{\rm kin}$ for the kinetic scheme at NLL (dashed) and NNLL (solid) on $S(\omega, 2.5\ \text{GeV})$ for $\mu_\Lambda = 1.0$ GeV. The dark lines correspond to using $m_b^{\rm kin}$ together with $\lambda_1^{\rm pole}$, while light lines use both $m_b^{\rm kin}$ and $\lambda_1^{\rm kin}$.

$u = 1/2$ renormalon from the pole mass, far less numerical analysis has been done on the low-order impact of the $u = 1$ renormalon in λ_1. If the low-order series is not yet influenced by the $u = 1$ renormalon, then schemes with an $\mathcal{O}(\alpha_s)$ correction may oversubtract, and not improve the perturbation series. In Fig. 14 we show that in our shape function analysis there is evidence that this is the case.[2] The dashed and solid curves are the NLL and NNLL results, respectively. The curves show $S(\omega, \mu_i = 2.5\ \text{GeV})$ with the kinetic mass scheme, but use either λ_1^{kin} (lighter solid and dashed curves) or λ_1 from Eq. (C2) (darker solid and dashed curves). In the λ_1^{kin} scheme the oscillatory behavior near the origin at both NLL and NNLL order is indicative of an oversubtraction.

Some understanding of the weakness of the $u = 1$ renormalon can be obtained from analytic computations. For Lorentz invariant regulators the $u = 1$ renormalon for λ_1 is invisible [60,61], namely, the ambiguity for λ_1 is smaller than dimensional analysis indicates. In perturbation theory renormalon ambiguities appear as a divergent series with terms $\sim n!\alpha_s^{n+1}$. However, the leading renormalon series $\sim n!\beta_0^n\alpha_s^{n+1}$ is absent, hence the renormalon ambiguity at lowest order in λ_1 is invisible [60]. Correspondingly, at one-loop order $Z_I = 0$ for Lorentz invariant regulators (even for a hard cutoff), and generically $Z_1 \propto C_A\alpha_s^2$ [61]. In the kinetic scheme the regulator is not Lorentz invariant, and hence not suppressed by invisibility. The same holds for definitions of λ_1 involving a lattice spacing regulator [60].

To avoid oversubtractions from λ_1 at low orders in perturbation theory, we would like to define a short distance scheme with $\delta\lambda_1 \sim \alpha_s^2$. This can be achieved by finding a scheme that is consistent with the suppression indicated by the invisible renormalon. To construct an invisible scheme for λ_1 we define

$$\lambda_1^{\text{i}}(R) = \lambda_1 - \delta\lambda_1^{\text{i}}(R), \tag{C3}$$

where the series in α_s is obtained by evaluating the matrix element

$$\delta\lambda_1^{\text{i}}(R) = \langle b_v|\bar{b}_v(iD_\perp)^2 b_v|b_v\rangle|_R. \tag{C4}$$

Here, R is a Lorentz invariant hard cutoff UV regulator, ensuring that $\delta\lambda_1^{\text{i}}(R) \sim R^2\alpha_s^2$. The definition in Eq. (C3) states that the invisible scheme $\lambda_1^{\text{i}}(R)$ is the kinetic energy of the b quark in the B meson minus the free kinetic energy of the b quark. Since the $\mathcal{O}(\Lambda_{\text{QCD}}^2)$ ambiguity in λ_1 is a UV effect caused by the mixing of the kinetic operator into $\bar{b}_v b_v$, it is the same for the B meson and b quark states, and cancels out in the difference. This can be seen explicitly by using Eq. (C1) and noting that our states are normalized so that $\langle B_v|\bar{b}_v b_v|B_v\rangle = \langle b_v|\bar{b}_v b_v|b_v\rangle = 1$. The $\mathcal{O}(\Lambda_{\text{QCD}}^2)$ ambiguity is universal to the definition of λ_1 and independent of R. Although a precise definition of R is needed to define the scheme, the $u = 1$ renormalon ambiguity cancels out in $\lambda_1 - \delta\lambda_1^{\text{i}}$ for any such regulator. We adopt a definition that allows us to use the computation in Ref. [61], where it was shown that $Z_1 \neq 0$ at $\mathcal{O}(\alpha_s^2)$ in a Lorentz invariant cutoff scheme. We define

$$\begin{aligned}\delta\lambda_1^{\text{i}} &= \lim_{v'\to v} A_{vv'}(0,0)|_R \\ &= \lim_{v'\to v}\int_0^R\int_0^R \frac{dwdw'}{(2\pi i)^2 ww'}\,\text{Disc}_w\,\text{Disc}_{w'}A_{vv'}(w,w'),\end{aligned} \tag{C5}$$

where

$$A_{vv'}(v\cdot k, v'\cdot k') = \frac{3\langle b_{v'}(k')|\bar{b}_{v'}v_\mu v'_\nu igG^{\mu\nu}b_v|b_v(k)\rangle}{(v\cdot v')^2 - 1}, \tag{C6}$$

and as usual the discontinuity of a function is given by $\text{Disc}_w f(w) = \lim_{\epsilon\to 0}[f(w + i\epsilon) - f(w - i\epsilon)]$. Note that it is sufficient to consider the $\bar{b}_{v'}igG^{\mu\nu}b_v$ operator due to the virial theorem in HQET, which relates $\lim_{v'\to v}A_{vv'}(0,0)$ to the corresponding matrix element of the kinetic energy operator in Eq. (C4). The result for the cutoff matrix element from Ref. [61] implies

$$\delta\lambda_1^{\text{i}}(R) = R^2 C_F C_A\left(\frac{\pi^2}{3} - 1\right)\frac{\alpha_s^2(\mu)}{4\pi^2} = 0.232R^2\alpha_s^2(\mu). \tag{C7}$$

Equation (C7) gives the relation of the invisible λ_1^{i} to the HQET λ_1 in Eq. (C2), which was used in the text. We use $R = 1$ GeV as our default value. Equations (C3) and (C5) provide a μ independent definition for $\lambda_1^{\text{i}}(R)$, so the μ dependence in $\alpha_s^2(\mu)$ will cancel against a higher order $R^2\alpha_s^3(\mu)\ln(\mu/R)$ term in $\delta\lambda_1^{\text{i}}(R)$.

[2]This observation relies on our use of $F_1(\omega) = \hat{F}(\omega)$ in Eq. (33) to determine $\delta C_0(\omega)$. It would be interesting to explore if a different choice would change the conclusions drawn from Fig. 14.

[1] M. Neubert, Phys. Rev. D **49**, 3392 (1994); **49**, 4623 (1994).

[2] I. I. Y. Bigi, M. A. Shifman, N. G. Uraltsev, and A. I. Vainshtein, Int. J. Mod. Phys. A **9**, 2467 (1994).

[3] K. S. M. Lee, Z. Ligeti, I. W. Stewart, and F. J. Tackmann, Phys. Rev. D **74**, 011501(R) (2006).

[4] K. S. M. Lee and I. W. Stewart, Phys. Rev. D **74**, 014005 (2006).

[5] M. Misiak *et al.*, Phys. Rev. Lett. **98**, 022002 (2007), and references therein.

[6] S. Chen *et al.* (CLEO Collaboration), Phys. Rev. Lett. **87**, 251807 (2001).

[7] K. Abe *et al.* (Belle Collaboration), arXiv:0804.1580; P. Koppenburg *et al.* (Belle Collaboration), Phys. Rev. Lett. **93**, 061803 (2004).

[8] B. Aubert *et al.* (*BABAR* Collaboration), Phys. Rev. D **77**, 051103(R) (2008); Phys. Rev. Lett. **97**, 171803 (2006); Phys. Rev. D **72**, 052004 (2005).

[9] B. Aubert *et al.* (*BABAR* Collaboration), arXiv:hep-ex/0408068; K. Tackmann (*BABAR* Collaboration), arXiv:0801.2985.

[10] C. W. Bauer, Z. Ligeti, M. Luke, A. V. Manohar, and M. Trott, Phys. Rev. D **70**, 094017 (2004); C. W. Bauer, Z. Ligeti, M. Luke, and A. V. Manohar, Phys. Rev. D **67**, 054012 (2003).

[11] O. Buchmüller and H. Flächer, Phys. Rev. D **73**, 073008 (2006).

[12] E. Barberio *et al.* (Heavy Flavor Averaging Group), arXiv:0704.3575, and updates at http://www.slac.stanford.edu/xorg/hfag/.

[13] C. Balzereit, T. Mannel, and W. Kilian, Phys. Rev. D **58**, 114029 (1998).

[14] S. W. Bosch, B. O. Lange, M. Neubert, and G. Paz, Nucl. Phys. **B699**, 335 (2004).

[15] A. K. Leibovich, I. Low, and I. Z. Rothstein, Phys. Rev. D **61**, 053006 (2000).

[16] A. K. Leibovich, I. Low, and I. Z. Rothstein, Phys. Lett. B **486**, 86 (2000).

[17] A. H. Hoang, Z. Ligeti, and M. Luke, Phys. Rev. D **71**, 093007 (2005).

[18] B. O. Lange, J. High Energy Phys. 01 (2006) 104.

[19] C. W. Bauer, Z. Ligeti, and M. E. Luke, Phys. Lett. B **479**, 395 (2000); Phys. Rev. D **64**, 113004 (2001).

[20] A. H. Hoang and I. W. Stewart, Phys. Lett. B **660**, 483 (2008).

[21] C. W. Bauer and A. V. Manohar, Phys. Rev. D **70**, 034024 (2004).

[22] M. Neubert, Eur. Phys. J. C **40**, 165 (2005).

[23] T. Becher and M. Neubert, Phys. Rev. Lett. **98**, 022003 (2007).

[24] G. P. Korchemsky and G. Sterman, Phys. Lett. B **340**, 96 (1994).

[25] C. W. Bauer, D. Pirjol, and I. W. Stewart, Phys. Rev. D **65**, 054022 (2002).

[26] T. Mannel and F. J. Tackmann, Phys. Rev. D **71**, 034017 (2005).

[27] F. J. Tackmann, Phys. Rev. D **72**, 034036 (2005).

[28] B. O. Lange, M. Neubert, and G. Paz, Phys. Rev. D **72**, 073006 (2005).

[29] W. M. Yao *et al.* (Particle Data Group), J. Phys. G **33**, 1 (2006), and 2007 partial update for the 2008 edition.

[30] A. H. Hoang, Z. Ligeti, and A. V. Manohar, Phys. Rev. Lett. **82**, 277 (1999); Phys. Rev. D **59**, 074017 (1999); A. H. Hoang and T. Teubner, Phys. Rev. D **60**, 114027 (1999).

[31] A. Czarnecki, K. Melnikov, and N. Uraltsev, Phys. Rev. Lett. **80**, 3189 (1998); Phys. Rev. D **57**, 1769 (1998); the $\alpha_s^2\beta_0$ part of what later became $\lambda_1^{\rm kin}$ was first obtained in: A. Kapustin, Z. Ligeti, M. B. Wise, and B. Grinstein, Phys. Lett. B **375**, 327 (1996).

[32] S. Fleming, A. H. Hoang, S. Mantry, and I. W. Stewart, Phys. Rev. D **77**, 114003 (2008).

[33] F. De Fazio and M. Neubert, J. High Energy Phys. 06 (1999) 017.

[34] P. Gambino, P. Giordano, G. Ossola, and N. Uraltsev, J. High Energy Phys. 10 (2007) 058.

[35] M. Abramowitz and I. A. Stegun, *Handbook of Mathematical Functions* (Dover, New York, 1964); for other proposed expansions, see, e.g.: A. H. Hoang and R. Hofmann, Phys. Rev. D **67**, 054024 (2003).

[36] C. W. Bauer, M. E. Luke, and T. Mannel, Phys. Rev. D **68**, 094001 (2003).

[37] A. K. Leibovich, Z. Ligeti, and M. B. Wise, Phys. Lett. B **539**, 242 (2002).

[38] C. W. Bauer, M. Luke, and T. Mannel, Phys. Lett. B **543**, 261 (2002).

[39] K. S. M. Lee and I. W. Stewart, Nucl. Phys. **B721**, 325 (2005).

[40] A. Kapustin, Z. Ligeti, and H. D. Politzer, Phys. Lett. B **357**, 653 (1995).

[41] S. J. Lee, M. Neubert, and G. Paz, Phys. Rev. D **75**, 114005 (2007).

[42] K. S. M. Lee, Phys. Rev. D **78**, 013002 (2008).

[43] M. Beneke, F. Campanario, T. Mannel, and B. D. Pecjak, J. High Energy Phys. 06 (2005) 071.

[44] M. Trott and A. R. Williamson, Phys. Rev. D **74**, 034011 (2006).

[45] J. R. Andersen and E. Gardi, J. High Energy Phys. 01 (2006) 097.

[46] U. Aglietti, F. Di Lodovico, G. Ferrera, and G. Ricciardi, arXiv:0711.0860.

[47] M. Neubert, Phys. Rev. D **72**, 074025 (2005).

[48] K. S. M. Lee, Z. Ligeti, I. W. Stewart, and F. J. Tackmann, Phys. Rev. D **75**, 034016 (2007).

[49] K. G. Chetyrkin, M. Misiak, and M. Münz, Phys. Lett. B **400**, 206 (1997); **425**, 414 (1998).

[50] C. W. Bauer, S. Fleming, D. Pirjol, and I. W. Stewart, Phys. Rev. D **63**, 114020 (2001).

[51] I. R. Blokland, A. Czarnecki, M. Misiak, M. Slusarczyk, and F. Tkachov, Phys. Rev. D **72**, 033014 (2005); K. Melnikov and A. Mitov, Phys. Lett. B **620**, 69 (2005).

[52] A. Ali, B. D. Pecjak, and C. Greub, Eur. Phys. J. C **55**, 577 (2008).

[53] T. Becher and M. Neubert, Phys. Lett. B **637**, 251 (2006).

[54] T. Becher and M. Neubert, Phys. Lett. B **633**, 739 (2006).

[55] G. P. Korchemsky and A. V. Radyushkin, Nucl. Phys. **B283**, 342 (1987).

[56] S. Moch, J. A. M. Vermaseren, and A. Vogt, Nucl. Phys. **B688**, 101 (2004).

[57] G. P. Korchemsky and G. Marchesini, Nucl. Phys. **B406**, 225 (1993).

[58] E. Gardi, J. High Energy Phys. 02 (2005) 053.

[59] A. Jain, I. Scimemi, and I. W. Stewart, Phys. Rev. D **77**, 094008 (2008).
[60] G. Martinelli, M. Neubert, and C. T. Sachrajda, Nucl. Phys. **B461**, 238 (1996).
[61] M. Neubert, Phys. Lett. B **393**, 110 (1997).
[62] M. E. Luke and A. V. Manohar, Phys. Lett. B **286**, 348 (1992).
[63] M. Beneke, V. M. Braun, and V. I. Zakharov, Phys. Rev. Lett. **73**, 3058 (1994); M. E. Luke, A. V. Manohar, and M. J. Savage, Phys. Rev. D **51**, 4924 (1995); M. Neubert and C. T. Sachrajda, Nucl. Phys. **B438**, 235 (1995).
[64] I. I. Y. Bigi, M. A. Shifman, N. G. Uraltsev, and A. I. Vainshtein, Phys. Rev. D **52**, 196 (1995).